Journal of Great Lakes Research 49 (2023) 406–421

Contents lists available at ScienceDirect

Journal of Great Lakes Research

journal homepage: www.elsevier.com/locate/ijglr

What role does stratification play during winter in wind-induced exchange between the multi-depth basins of a large lake (Lake Geneva)?

Rafael Sebastian Reiss *, Ulrich Lemmin, David Andrew Barry

Ecological Engineering Laboratory (ECOL), Institute of Environmental Engineering (IIE), Faculty of Architecture, Civil and Environmental Engineering (ENAC), Ecole Polytechnique Fédérale de Lausanne (EPFL), 1015 Lausanne, Switzerland

ARTICLE INFO

Article history:
Received 1 August 2022
Accepted 26 January 2023
Available online 13 February 2023
Communicated by: Jay Austin

Keywords:
Upwelling
Interbasin exchange
Coriolis force
Deepwater renewal
Momentum budget
Winter stratification

ABSTRACT

Detailed studies of wind-driven interbasin exchange in lakes, focusing on the underlying driving forces and how they are affected by stratification, are presently lacking. We therefore investigated how stratification modifies wind-induced exchange between the *Petit Lac* (*PL*) (depth 75 m) and *Grand Lac* (*GL*) (depth 309 m) basins of Lake Geneva in winter, using field observations, 3D hydrodynamic modeling and particle tracking. Early, weakly-stratified (December) and late, fully-mixed (March) winter conditions in the *PL* were compared for a typical, strong along-axis wind forcing. During early winter, two-layer exchange develops between the basins, with downwind surface outflow into the *GL* balanced by intense bottom inflow of deep, cold hypolimnetic *GL* water into the *PL* which is enhanced by baroclinic pressure gradients caused by upwelling in the *GL*. Furthermore, the transversal water-level setup generates barotropic pressure gradients that balance Coriolis force acting on the outflow. This produces unidirectional along-wind epilimnion currents that strengthen interbasin exchange. In late winter, with the thermocline deeper than the *PL* bottom, upwelling in the *GL* does not reach the confluence and baroclinicity plays no role, resulting in weaker exchange currents with a depth-veering structure in the upper layers due to Coriolis force. In late winter, interbasin exchange decreases by 50 %, is more local, affects only waters near the confluence, and is more horizontal, with no deepwater upwelling from the *GL*. Our results suggest that prolonged winter stratification due to global warming will make wind-induced hypolimnetic interbasin-upwelling an increasingly important deepwater renewal process in large multi-depth basin lakes.

Introduction

Horizontal transport and mixing processes in lakes, induced by wind and affected by thermal stratification, can cause the vertical redistribution of biogeochemical tracers such as dissolved oxygen and nutrients. This in turn can significantly impact water quality. In multi-basin lakes, horizontal interbasin gradients in water quality can exist for a number of reasons, e.g., due to localized nutrient loading (Lake Michigan: Hamidi et al., 2015), differences in the thermal structure and productivity (Lake Erie: Bartish, 1987), or different seasonal mixing regimes in adjacent basins of different depths (Lake Garda: Salmaso, 2005; Lake Geneva: CIPEL, 2016). Consequently, exchange processes between sub-basins, especially between their hypolimnia, can have significant negative and positive ecological consequences, for example, by upwelling hypoxic waters (Jabbari et al., 2021, 2019), or by ventilating deep layers (Ahrnsbrak and Wing, 1998; Boyce et al., 1980; Reiss et al., 2022), respectively.

Wind stress is an important driver for interbasin exchange in stratified lakes. It can act directly by two-way advective exchange, where the downwind surface drift towards one basin is balanced by a hypolimnetic counterflow into the other basin (Laval et al., 2008; Niu et al., 2015; Reiss et al., 2022), or indirectly through internal wave pumping (Flood et al., 2020; Imam et al., 2013; Umlauf and Lemmin, 2005; van Senden and Imboden, 1989) and geostrophic adjustment processes after the relaxation of coastal upwelling fronts (Jabbari et al., 2021). Coastal upwelling near the junction between basins can also produce interbasin density gradients that drive exchange flows (Lawrence et al., 2004; Liu et al., 2018; Schertzer et al., 2008).

Density-driven interbasin exchange across constrictions, for example, through narrow channels or over sills, has been widely studied with simplified, steady analytical models, e.g., based on inviscid internal hydraulic theory (Hamblin, 1998; Hogg et al., 2001; Lawrence et al., 2004; Rueda and Cowen, 2005). However,

* Corresponding author.
E-mail address: rafael.reiss@epfl.ch (R.S. Reiss).

https://doi.org/10.1016/j.jglr.2023.02.005
0380-1330/

unsteady effects resulting from the interplay of realistic wind forcing, the Earth's rotation and irregular bathymetry cannot be represented by such simplified models (e.g., Rueda and Cowen, 2005). Furthermore, large, deep lakes are often composed of sub-basins with different depths, but with relatively similar widths that allow an almost unrestricted exchange flow between the basins. For this case, detailed studies of direct wind-driven interbasin exchange, focusing on the underlying driving forces and how they are affected by stratification, are presently lacking.

Overall, stratification plays an important role in wind-induced interbasin exchange in lakes, not only by imposing a two-layer current structure, but also by producing baroclinic pressure gradients between the basins. Rueda et al. (2008) studied contaminant transport in a shallow (mean depth 8 m), polymictic, large, multi-basin lake and found that under stratified conditions, wind stress and baroclinic pressure gradients acted together to enhance the exchange through a narrow passage between two basins. On a larger scale, Anderson and Schwab (2017) investigated the exchange between Lake Michigan and Lake Huron through the 6-km wide and 30 to 80-m deep Straits of Mackinac, which is dominated year-round by a barotropic Helmholtz mode, i.e., a special type of a surface seiche (e.g., Roberts et al., 2019) due to regional-scale meteorology (see also Anderson and Schwab, 2013). They showed that during the stratified period a bidirectional baroclinic two-layer exchange develops that can be modified or reversed by local winds.

Global warming continues to weaken convective cooling during winter, thereby altering the long-term thermal structure of lakes, for example, by reducing the maximum mixed-layer depth of deep monomictic or oligomictic lakes and by extending the stratification period (e.g., Lemmin and Amouroux, 2013; Mesman et al., 2021; Perroud and Goyette, 2012). This raises the important question of how these expected stratification changes will impact wind-driven interbasin exchange, for example, by modulating its strength or by suppressing vertical exchange and hypolimnetic upwelling between the basins.

Recently, Reiss et al. (2022) investigated the wind-driven exchange between the two basins of different depths and widths of Lake Geneva during early winter when the lake was still weakly stratified. They demonstrated that regular along-axis winds generate a "current loop," where deep, hypolimnetic waters from the deep basin first upwell and penetrate far into the shallow basin, carried by strong bottom currents, replacing ~50 % of the shallow basin volume, before descending back into the hypolimnion of the deep basin after the wind ceased. This current loop provides an as yet overlooked mechanism for hypolimnetic-epilimnetic exchange and deepwater renewal in the deep basin.

In the present study, we will examine how the wind-driven exchange between the two basins of Lake Geneva is modified by the presence or absence of thermal stratification during winter (see Fig. 1b), combining field observations, three-dimensional (3D) hydrodynamic modeling and particle tracking. In particular, we will detail and quantify for the first time in a large deep lake, the driving forces behind wind-driven interbasin exchange under stratified (December; early winter) and unstratified (March; late winter) conditions using model-based momentum budgets, highlighting the role of baroclinicity and rotational effects. Furthermore, the implications of changes in stratification for the flushing of the shallow basin and the vertical exchange between the basins are evaluated, both being potential deepwater renewal processes for the deep basin. The following questions are addressed:

- How are the axial and transversal circulation patterns at the "confluence" between the basins affected by stratification? Does this affect the strength of the interbasin exchange?

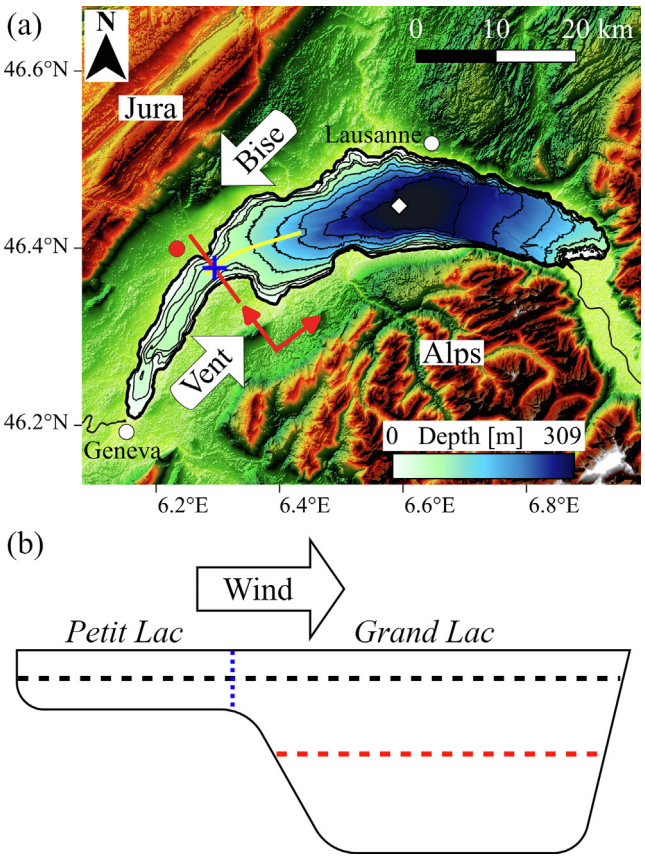

Fig. 1. (a) Bathymetric map of Lake Geneva including the surrounding topography. The white arrows indicate the direction of the two strong dominant winds called *Bise* and *Vent* that frequently blow over large areas of the lake, channeled by the Alps and Jura mountains. The red line approximately delimits the confluence between the two basins composing Lake Geneva, i.e., the small *Petit Lac* and the large *Grand Lac*. The blue cross in the center of the confluence shows the mooring location. Meteorological data were recorded at the MeteoSwiss station in Nyon (red circle) and the white diamond marks the location of the CIPEL monitoring station SHL2 (depth 309 m). Depth is given in meters in the colorbar legend and by the isobath contours (0, 25, 50, 60, 100, 150, 200, 250, 300 m). The model results shown in Figs. 5 and 6 were obtained along the yellow and red lines. The red arrows indicate the positive transversal and axial directions referred to in the momentum budget analysis. (b) Cross-section of the two basins (vertically exaggerated) showing bathymetry and stratification conditions. Horizontal black dashed line: thermocline depth during early winter. Red dashed line: thermocline depth during late winter. Vertical blue dashed line: mooring location (corresponding to the blue cross in panel a). (For interpretation of the references to color in this figure legend, the reader is referred to the web version of this article.)

- How is the wind-induced circulation between the basins modified by the Coriolis force? Is there a difference during stratified and fully-mixed conditions?
- How does stratification modify the vertical structure of the exchange? Does hypolimnetic upwelling between the basins occur when the shallower basin is fully mixed?

Details of the mooring setup and additional figures that complement the text are provided in the Electronic Supplementary Material (ESM).

Material and methods

Study site

Lake Geneva (local name: *Lac Léman*), Western Europe's largest freshwater lake, is an oligomictic, perialpine lake located between Switzerland and France. It has a volume of 89 km^3, a surface area of

580 km^2, and a theoretical residence time of 11 y (CIPEL, 2019). The lake has a total length of 73 km and is composed of two basins: the large, eastern *Grand Lac* (maximum width 14 km and depth 309 m), and the small, western *Petit Lac* (maximum width 5 km and depth 75 m), joined at a 3.5-km wide and 65-m deep "confluence" (Fig. 1a). The shallow *Petit Lac* annually destratifies completely, typically by early January, whereas the deeper *Grand Lac* remains weakly stratified throughout most seasons with the maximum mixing depth reaching 100 to 150 m in late February or early March. Occasionally, complete convective overturning in the *Grand Lac* occurs during severely cold winters (CIPEL, 2019).

The different mixing regimes in the two basins result in biochemical gradients between the deep layers of the basins, notably in dissolved oxygen (higher values in the *Petit Lac*) and nutrient concentrations (higher values in the *Grand Lac*) (e.g., CIPEL, 2016; Lavigne and Nirel, 2016). This implies that hypolimnetic exchange and mixing processes between the basins may have important ecological effects, since they can transport oxygen-rich waters from the shallow basin to the deep basin, or nutrients from the deep basin to the shallow basin.

Lake Geneva is bordered by the Alps in the south and the Jura mountains in the northwest. Two large-scale, strong wind fields that are guided by this topography dominate the region, namely the *Bise* coming from the northeast and the *Vent* from the southwest; both approximately aligned with the main axis of the *Petit Lac* (Graf and Prost, 1980; Lemmin and D'Adamo, 1996; Wanner and Furger, 1990). These winds are characterized by high wind speeds (5–15 m s^{-1}) often lasting for several days that considerably impact the lake's hydrodynamics, for example, by causing deep coastal upwelling (Reiss et al., 2020), wind-induced interbasin upwelling (Reiss et al., 2022) and enhanced interbasin exchange due to internal Kelvin waves (Umlauf and Lemmin, 2005).

Field observations

In the present study, data from a mooring deployed at 65-m depth in the center of the confluence between the *Petit Lac* and *Grand Lac* basins (Fig. 1a, blue cross) are used. The mooring was part of a larger field campaign carried out in winter 2018/2019 (see Reiss et al., 2022 for details). The mooring consisted of a bottom-mounted, upward-looking 300 kHz Teledyne-RDI Workhorse Sentinel Acoustic Doppler Current Profiler (ADCP), with a 10-m long thermistor line attached to the top of the ADCP frame. The measured currents were projected on the along- and cross-axis directions of the *Petit Lac*, hereinafter referred to as axial and transversal directions, respectively (Fig. 1a). Prior to the analysis, 2-h and 10-min moving averages were applied to the ADCP and thermistor data, respectively. The instrument settings are summarized in ESM Table S1.

The typical depth of the thermocline in Lake Geneva during early and late winter was inferred from Conductivity-Temperature-Depth (CTD) profiles provided by the Commission Internationale pour la Protection des Eaux du Léman (CIPEL, last accessed on 28 October 2022; Rimet et al., 2020) at the deepest point of the lake (309 m; SHL2 in Fig. 1a). Wind speed and direction were recorded every 10 min at a meteorological station located in Nyon, ~5 km northwest of the confluence (Fig. 1a), maintained by the Swiss National Weather and Climate Service (MeteoSwiss, last accessed on 28 October 2022).

Hydrodynamic model

The three dimensional (3D) hydrodynamic model used here is based on a hydrostatic version of the MITgcm code (Marshall et al., 1997), with a configuration similar to that employed by Cimatoribus et al. (2018) who studied nearshore boundary layer dynamics in Lake Geneva and also performed a detailed validation based on various field observations around the lake. The model was thereafter further validated and successfully applied to Lake Geneva to investigate the transport of inflowing water from the lake's main tributary, the Rhône River (Cimatoribus et al., 2019), wind-driven coastal upwelling during winter (Reiss et al., 2020), wind-induced interbasin exchange (Reiss et al., 2022), the effect of basin-scale circulation on river plume dynamics (Soulignac et al., 2021), submesoscale filaments in basin-scale gyres (Hamze-Ziabari et al., 2022), and submesoscale frontal slicks (Foroughan et al., 2022). In all these studies, the model results compared well with field measurements. Following Reiss et al. (2022), the domain was discretized by a uniform horizontal Cartesian grid with a resolution of 113 m and 100 size-varying z-layers, ranging from 30 cm at the surface to 2.8 m at the deepest point of the confluence and 4.8 m at the bottom of the *Grand Lac*. Realistic surface forcing for a typical winter *Vent* wind event was obtained from the COSMO-1 numerical weather model provided by MeteoSwiss (Voudouri et al., 2017).

To determine the effect of stratification alone on interbasin exchange, we ran two simulations, with identical external forcing but different initial lake temperature fields. Two initial temperature profiles were generated (Fig. 2), representing the lake's typical stratification in December and February/March based on long-term measurements (CIPEL, 2019), hereinafter referred to as early and late winter, respectively. In order to allow comparing the two simulations, we forced the model for both simulations with the COSMO wind for the period from 7 to 18 December 2018, which included a 2.5-d *Vent* wind event (from the southwest), with mean and maximum wind speeds of ~6 m s^{-1} and 11 m s^{-1}, respectively. As will be shown in the Results and Discussion section, the actual winds during the *Vent* event in December 2018 and in March 2019

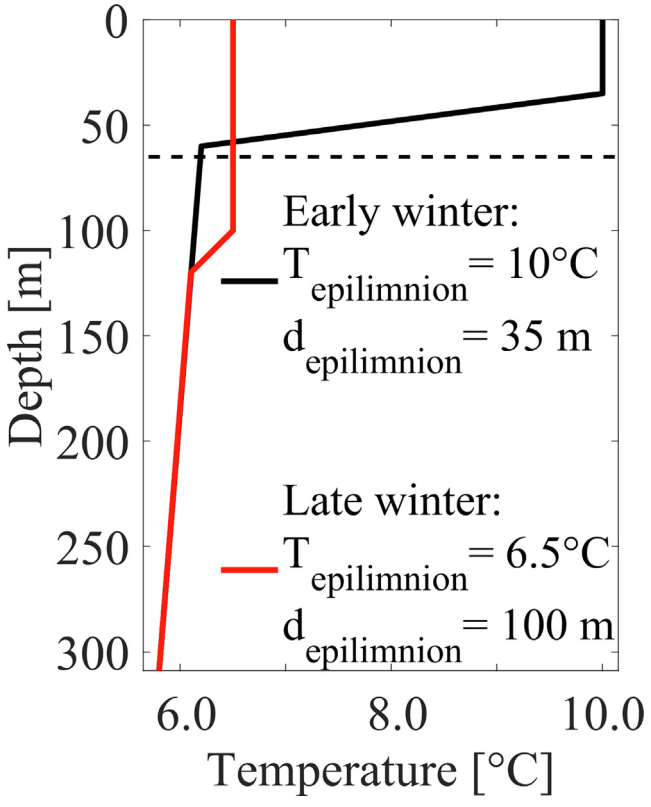

Fig. 2. Idealized temperature profiles representing the typical early (December; black line, epilimnion depth, $d_{epilimnion}$ of 35 m) and late (March; red line, $d_{epilimnion}$ of 100 m) winter stratification in Lake Geneva, used to initialize the 3D hydrodynamic model. The horizontal dashed line marks the maximum depth of the confluence. (For interpretation of the references to color in this figure legend, the reader is referred to the web version of this article.)

were comparable in duration and strength. For convenience, the MITgcm calendar was set such that the two simulations ran from 7 to 18 December (early winter) and from 7 to 18 March (late winter). The simulations were initialized with zero current velocity. Since strong, persistent wind stress rapidly induced a strong circulation, this initial condition did not noticeably affect the results, as was confirmed by comparison with model results that included a 3-month spin-up (cf. Reiss et al., 2022 for details on the spin-up simulation results).

Momentum budget

To shed light on the driving mechanisms behind the interbasin exchange under different stratification regimes, momentum balances at the confluence were analyzed (Fig. 1). The MITgcm model allows storing all terms of the momentum budget equations in both horizontal directions of the grid at each grid cell. The vector terms were linearly interpolated onto the vertical confluence transect and rotated to be aligned with the axial and transversal directions (see Field observations section and Fig. 1a). The horizontal momentum budget equation considered here takes the form (e.g., Vallis, 2017):

$$\frac{\partial_{\mathrm{h}}}{\partial t} = P_c + P_t + C + A + D \tag{1}$$

where $\mathbf{v}_{\mathrm{h}}$ are the horizontal components of the 3D velocity vector $\mathbf{v} = (\mathrm{u}, \mathrm{v}, \mathrm{w})$. $P_c = -g/\rho_0 \int_z^{\eta} \nabla \rho dz$ is the baroclinic and $P_t = -g\nabla\eta$ is the barotropic pressure gradient term, with reference density ρ_0, density ρ, gravitational acceleration g, free surface elevation η and depth z. $C = (f\mathrm{v}, -f\mathrm{u})$ is the Coriolis acceleration vector, with Coriolis parameter f, $A = (-(\mathbf{v}\cdot\nabla)\mathbf{v})_h$ is the nonlinear advection term (hereinafter referred to as the nonlinear term), and $D = \left(v_t \nabla^2 \mathbf{v}\right)_h$ represents the dissipation due to bulk and bottom friction, with turbulent (eddy) viscosity v_t. Note that the external forcing term acting on the surface cells (e.g., Cimatoribus et al., 2018), is not explicitly included since it is not relevant for the cell-wise momentum balances in the interior. Instead, the effect of the external forcing is included in the friction term D. The barotropic pressure gradient term was calculated based on the modeled surface elevation, whereas the remaining terms of Eq. (1) were directly derived from the MITgcm diagnostics module output (e.g., Brett et al., 2020).

Particle tracking

The particle tracking algorithm used here, implemented by Cimatoribus (2018) and based on the method described by Döös et al. (2013), was previously applied to Lake Geneva to study the transport of inflowing water from the lake's main tributary, the Rhône River (Cimatoribus et al., 2019), wind-driven coastal upwelling at the northern *Grand Lac* shore (Reiss et al., 2020), and wind-induced interbasin exchange between the *Grand Lac* and *Petit Lac* in weakly stratified early winter (Reiss et al., 2022).

The origin of the deep *Petit Lac* waters was traced by backward tracking of particles released in the bottom layers of the shallow basin. Particles were released every 4 h during the first 5 d of the wind event in a ~3-km × 5-km wide area near the confluence at every vertical grid point below 40-m depth (ESM Fig. S1), yielding a total of more than 200,000 particles. Increasing the number of particles by doubling the seeding frequency and increasing the vertical seeding resolution did not significantly affect the results of the particle tracking analysis, indicating their statistical robustness.

Results and Discussion

In this section, we first compare the field observations at the confluence during two *Vent* wind events with comparable speeds and duration under different stratification conditions, i.e., under weak stratification in December 2018 and under fully-mixed conditions in March 2019 (Fig. 1b). Then, we analyze and discuss in detail how stratification affects the *Vent*-induced circulation near the confluence using 3D hydrodynamic modeling and particle tracking results, again highlighting the differences between the different stratification regimes or showing similarities when they occur. To that aim, the model was initialized with two different temperature profiles representing the different stratification conditions during the two observation periods (Fig. 2), and forced in both cases with the wind field taken from the December *Vent* wind event.

Field observations

Fig. 3 summarizes the wind data measured at the MeteoSwiss Nyon station (for location, see Fig. 1a) and the currents and temperatures recorded at our mooring in the center of the confluence between the two basins (Fig. 1a, blue cross) during two typical *Vent* wind events from 8 to 10 December 2018 and from 9 to 11 March 2019. Full-depth current velocity and direction profiles for both periods are given in Fig. 4.

The two wind events were comparable in duration and strength, with overall mean wind speeds of 5.5 and 4.9 m s^{-1} and maximum hourly averages of 10.7 and 9.4 m s^{-1} in early and late winter, respectively. As is typical for *Vent* conditions, the wind fields were spatially relatively homogeneous and approximately aligned with the main axis of the *Petit Lac*, as shown by the COSMO-1 model wind fields (ESM Fig. S2). Prior to the early winter event, the thermocline was at ~35-m depth, with temperatures in the *Petit Lac* epilimnion and hypolimnion of ~10 °C and 6.3 °C, respectively. In March, on the other hand, temperatures in the *Petit Lac* were nearly homogeneous at ~6.5 °C, with a weak thermocline in the *Grand Lac* below 100-m depth (ESM Fig. S3).

In early winter (December), a two-layer flow pattern was established approximately half a day after the wind started with a reversal of current directions at the thermocline depth. The currents in the epilimnion were approximately aligned with the wind and flowed towards the *Grand Lac* (hereinafter referred to as outflow, Fig. 3d, e), and a countercurrent into the *Petit Lac* prevailed in the hypolimnion (hereinafter referred to as inflow, Fig. 3d, g). Current velocities in both layers exceeded 20 cm s^{-1}. However, the bottom layer currents were steadier and stronger, with maximum velocities above 27 cm s^{-1} (Figs. 3, 4). Even though the bottom inflow weakened after the wind stopped, it persisted for approximately another 1.5 d (ESM Fig. S4), enhancing the total volume exchange between the basins. The stronger bottom currents and sustained bottom inflow were due to axial baroclinic pressure gradients as will be further discussed below based on the model results. The flow in both the epilimnion and hypolimnion was vertically unidirectional; there was little variation in the current direction with depth in each layer (Fig. 4b). Shortly after the bottom inflow started, temperatures continuously decreased, reaching a minimum of 5.96 °C approximately 1.5 d after the wind had stopped. This temperature corresponds to water temperatures found at ~180-m depth as recorded at the CIPEL station SHL2 in December 2018 (ESM Fig. S3), and illustrates the upwelling of cold, hypolimnetic *Grand Lac* water into the shallow *Petit Lac* (cf. Reiss et al., 2022). The upwelling will be further discussed below based on particle tracking results.

In late winter (March), the currents at the confluence were weaker and less steady than in December, even though wind forc-

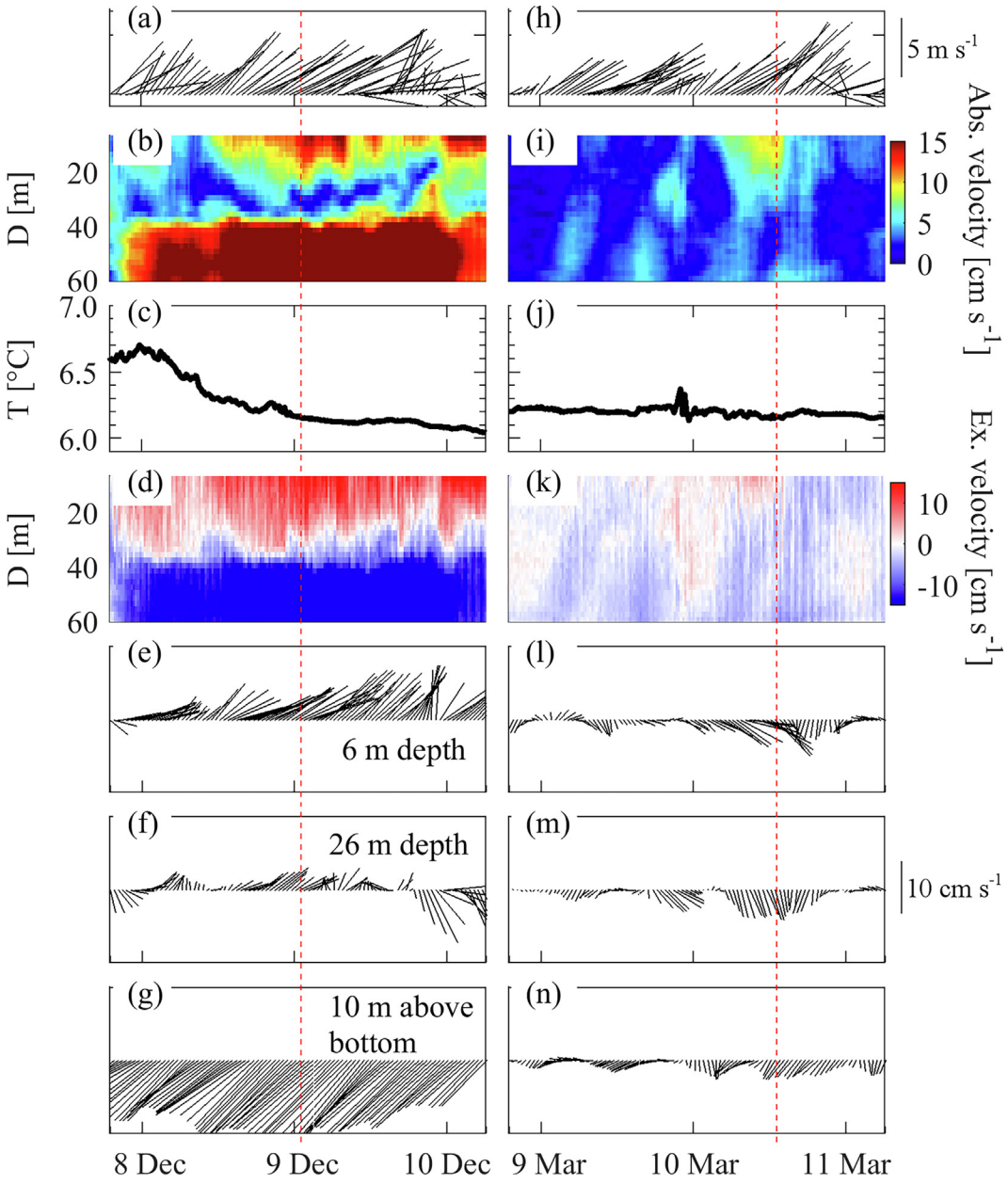

Fig. 3. Field data recorded from 8 to 10 December 2018 (left column) and from 9 to 11 March 2019 (right column). Hourly-averaged wind vectors (a, h) and mooring data (b-g, i-n). Absolute current velocity (b, i), depth-averaged temperature (T) in the bottom-most 10 m (D is depth) (c, j), "interbasin exchange velocity" (d, k), current velocity and direction at 6-m depth (e, l), 26-m depth (f, m), and 10 m above the bottom (g, n). Interbasin exchange velocities were obtained by projecting the velocity vectors onto a plane perpendicular to the confluence transect (Fig. 1a, red arrow). The colorbars give the magnitude of the absolute and interbasin exchange velocities. The scale of the wind and current quivers is the same for both periods and is given next to panels h and m. The quiver heads point in the direction of travel, with the positive *y*- and *x*-directions corresponding to north (0°) and east (90°), respectively. The red dashed lines mark the times of the velocity profiles shown in Fig. 4. Meteorological data were recorded at the MeteoSwiss station in Nyon (Fig. 1a, red circle). See Fig. 1a (blue cross) for mooring location. (For interpretation of the references to color in this figure legend, the reader is referred to the web version of this article.)

ing was comparable. The highest current velocities of ~10 cm s^{-1} were observed in the topmost ADCP bin at ~6-m depth, coinciding with the period of maximum wind speeds. The time history of the measured velocities showed significant variability and no two-layer structure. Different from the early winter situation: (i) the upper layer currents were more often directed towards the *Grand Lac* than those in the intermediate layers, (ii) they were never aligned with the wind, but instead were deflected ~30° to 90° to the right, and (iii) the rightward deflection increased with depth, producing a veering current structure resembling that of an Ekman spiral (Figs. 3h-n and 4).

The temperatures in the lower layer changed little throughout the wind event, except for small fluctuations at ~23:00 (local time) on 9 March. These fluctuations were associated with increased current velocities in the middle of the water column (Fig. 3i-k) and were most pronounced at the topmost thermistor, 10 m above the lakebed, suggesting the temporary downwelling of slightly warmer surface waters. The temperatures 1 m above the lakebed remained within ± 0.03 °C during the entire period (not shown). Altogether, the observations during late winter showed no signs of upwelling of cold, deep *Grand Lac* water into the *Petit Lac* (compare Fig. 3c and j; discussed further below based on the model

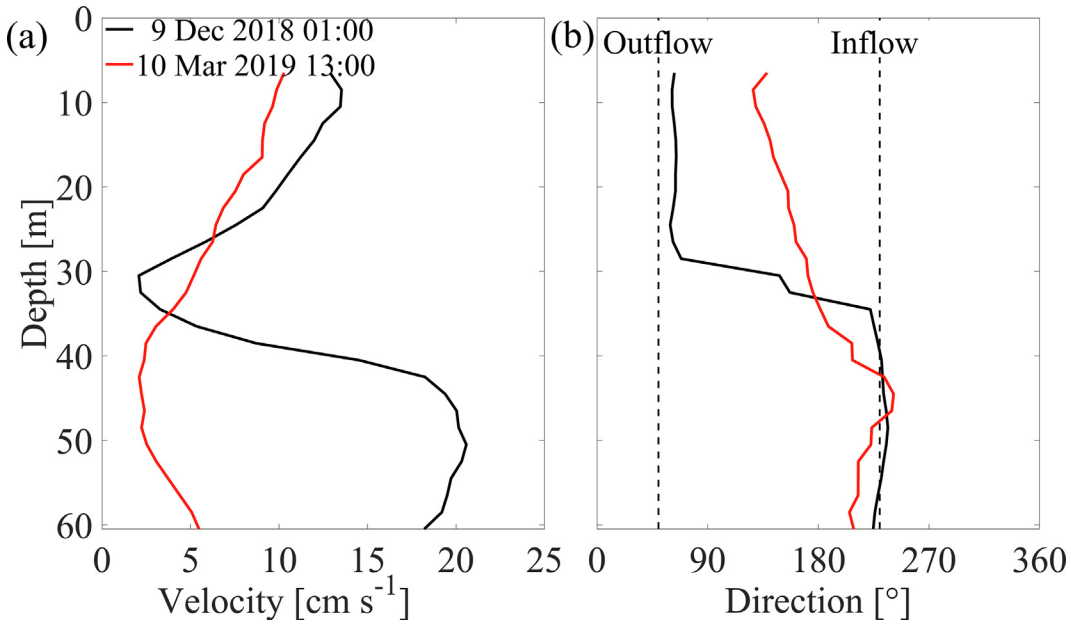

Fig. 4. Current velocity (a) and direction (b) recorded at the confluence center (Fig. 1a, blue cross) during the *Vent* wind events in December 2018 (solid black lines) and March 2019 (red lines). The exact dates are given in the legend in (a). The black dashed lines mark the outflow and inflow directions. The times of the profiles are marked in Fig. 3 by the red dashed lines. (For interpretation of the references to color in this figure legend, the reader is referred to the web version of this article.)

results). Furthermore, the currents were significantly weaker than in early winter, with their vertical structure in the upper layers apparently strongly influenced by the Coriolis force.

Model results

The field observations above showed that the *Vent*-induced flow patterns at the confluence in early stratified winter were markedly different from those in late destratified winter. In the following sections, the impact of stratification on the temporal development of the wind-induced circulation at the confluence is further investigated using 3D hydrodynamic model results. Model results (temperature, velocities, and momentum budget terms) were analyzed based on 4-h moving averages.

Temperature field

Fig. 5 presents the modeled temperatures near the confluence along the transect marked in Fig. 1a, before and 1.5 d after the wind started. The latter approximately corresponds to the time of the measured current velocity profiles at the confluence center shown in Fig. 4 and was chosen to allow for rotational effects to be fully developed (local inertial period ~16.5 h). In early winter, the lake was stratified, with a thermocline at ~35-m depth. By late winter, the thermocline had descended to ~100-m depth, resulting in a fully-mixed *Petit Lac* and a hypolimnion confined to the *Grand Lac* (Fig. 5). The initial temperature fields below 120-m depth were identical in both simulations (dashed 6.1 °C isotherm lines in Fig. 5; see also Fig. 2).

Under both stratification regimes, the *Vent* wind coming from the southwest caused upward tilting of the isotherms towards the western end of the *Grand Lac* near the confluence. This will

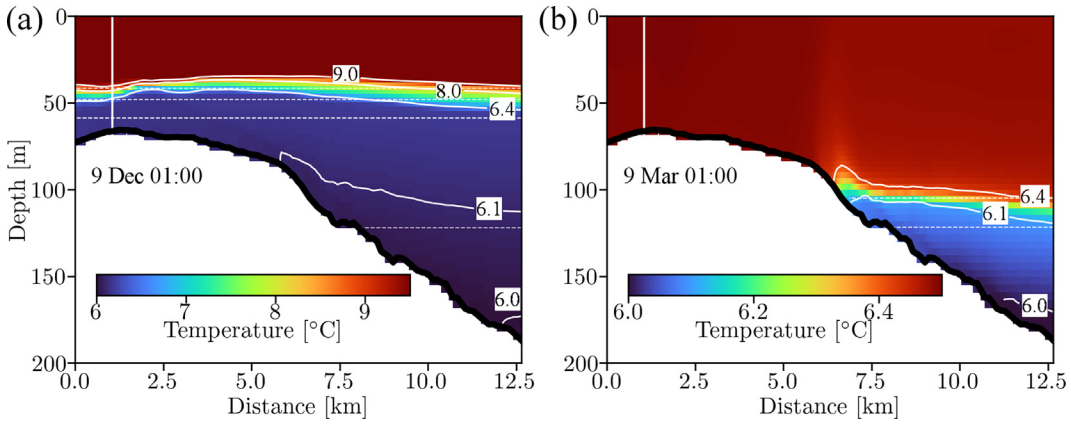

Fig. 5. Modeled temperatures along a curved transect, approximately following the central axis of the lake and perpendicular to the confluence (Fig. 1a, yellow line), during early (a) and late (b) winter, ~1.5 d after the wind started (corresponding to times marked by the red dashed lines in Fig. 3). The white vertical lines mark the location of the confluence center, where the mooring was deployed (Fig. 1a, blue cross). Temperatures are given by the colorbars (note the different ranges in a and b). Selected isotherms are depicted by the solid white lines (see isotherm labels for values). The white dashed lines show the corresponding initial horizontal position of the isotherms before the wind started (compare with profiles in Fig. 2). Distance is given along the transect starting at its southwestern end, ~500 m west of the confluence (Fig. 1a, yellow line). Compare with velocity profiles in Fig. 4. (For interpretation of the references to color in this figure legend, the reader is referred to the web version of this article.)

hereinafter be referred to as upwind upwelling in the *Grand Lac*, since it resembles wind-driven upwelling that occurs at the upwind end of a closed basin (e.g., Laval et al., 2008).

In early winter, the maximum upward displacement of the isotherms occurred ~2 to 4 km east of the confluence in the *Grand Lac*. Further westwards, in the *Petit Lac*, the isotherms were also displaced upwards compared to pre-wind conditions, but to a lesser extent (Fig. 5a). The upwind upwelling in the *Grand Lac* and the discontinuous upward tilt of the isotherms across the confluence are due to the different widths of the two basins; thus, the wind-induced surface drift in the narrow *Petit Lac* was not sufficient to balance that in the wider *Grand Lac*. As a result, a horizontal current divergence east of the confluence caused upwind upwelling in the *Grand Lac*, similar to what has been observed in Lake Constance (Appt et al., 2004). This was confirmed by comparing the net downwind transport through a north–south transect at the confluence with an adjacent transect in the western *Grand Lac*.

Due to the deeper thermocline in late winter, the two basins were baroclinically decoupled, and the upwind upwelling was limited to the *Grand Lac* below the confluence (Fig. 5b). Consequently, the shallow *Petit Lac* basin remained well-mixed throughout the entire wind event, as discussed in the Field observations section.

Development of the axial and transversal circulations at the confluence

To investigate the temporal development leading to the measured bottom-intensified inflow and unidirectional outflow in early winter, as well as the veering surface currents in late winter (Fig. 4), the following three phases are considered: (i) initialization phase: ~4h after the wind started, (ii) adjustment phase: ~12 h after the wind started, and (iii) fully-developed circulation: ~1.5 d after the wind started. Note that the selected times do not necessarily mark the start or end of each phase, but instead are representative for the prevailing currents. Since the focus of this study is on wind-induced interbasin exchange, the circulation at the confluence between the two basins is discussed here. Important implications for the basin-scale circulation will be further examined below based on particle tracking simulations.

The modeled currents at the confluence during the three phases, both in the axial (in- and outflow; blue and red colors) and transversal (cross-shore flow at the confluence; black arrows) directions are shown in Fig. 6. Full-depth current velocity and direction profiles at the confluence center are given in Fig. 7 with the corresponding profiles of the axial and transversal velocity components presented in ESM Fig. S5. Hereinafter, unless stated otherwise, rightward and leftward transversal currents are with respect to the outflow direction into the *Grand Lac*, that is, when looking into the page in Fig. 6.

Initialization phase. A few hours after the wind started, the current patterns were similar under both stratification regimes (Fig. 6a, b). The strong wind stress initiated an outflow towards the *Grand Lac* in the uppermost 10 m, which was balanced by a weaker inflow distributed over the entire depth range below 10 m. The currents were strongest near the surface, reaching 10 cm s^{-1} in early winter and 8 cm s^{-1} in late winter. A weaker secondary circulation developed in the transversal direction, with the highest velocities ~1.5 cm s^{-1} near the surface (see also ESM Fig. S5a, b). The transversal currents in the upper layers were oriented to the right (towards the southern shore) and were balanced by weaker opposing currents towards the northern shore in the layers below (Fig. 6a, b). Under both stratification regimes, the net currents in the upper layers at the center of the confluence displayed a spiraling motion, i.e., with increasing depth, magnitudes decreased and directions veered to the right (Fig. 7, black curves). In early winter, the isotherms began to tilt upward towards the northern shore, indicating the onset of Coriolis force-induced coastal upwelling (Fig. 6a).

Adjustment phase. As the wind stress continued, both the axial and transversal circulations strengthened, and clear differences between the two stratification regimes emerged (Fig. 6c, d). In early winter, the stratification imposed a two-layer pattern with a strong, bottom-intensified inflow in the hypolimnion that balanced the downwind epilimnetic outflow. The thermocline continued to tilt upwards towards the northern shore (Figs. 6c and 7a, b). In late winter, however, the downwind outflow was more pronounced in the shallow nearshore regions, where it extended over the entire water column. Away from the shores, the outflow was limited to the uppermost 10 m and a weak upwind inflow prevailed in most of the transect. This resulted in a dome-shaped zero isotach (Figs. 6d and 7c). Due to the stronger and deeper-reaching outflow in early winter, the net currents in the epilimnion gradually approached a more unidirectional structure, whereas their depth-veering structure remained unchanged in late winter (Fig. 7b, d).

In both cases, the transversal circulation resembled a horizontal clockwise vortical motion, with near-zero velocities in the center, leftward currents in the lower layers balancing the rightward near-surface currents, and downwelling at the right and upwelling at the left boundaries. This transversal vortex was confined to the epilimnion when stratification was present, whereas it spanned the entire water column in the fully-mixed case (Fig. 6c, d). The strength of the transversal secondary circulation was comparable in both cases.

Fully-developed circulation. In early winter, the two-layer pattern strengthened and both inflowing and outflowing velocities exceeded 20 cm s^{-1}. The net currents in both layers were nearly unidirectional and aligned with the axial direction, with a sharp current reversal at about the thermocline depth (Figs. 6e and 7a, b). Furthermore, the upwelling at the northern shore continued, with the 9 °C isotherm, initially at 42-m depth, reaching ~10-m depth. This illustrates that the bottom inflow was strongly modified by the Coriolis force, as will be discussed below in the momentum budget analysis (see Reiss et al., 2022 for details on the coastal upwelling dynamics in the *Petit Lac* basin).

In late winter, the dome-shaped zero-isotach developed into an inverse U-shape. Downwind currents were strongest in the shallow nearshore regions, with the interior dominated by weaker upwind inflow. At the confluence center, the upper layer currents maintained their depth-veering structure, confining the outflow to the uppermost 5 to 10 m. The transversal vortex grew stronger (Figs. 6f and 7c, d). In both cases, the modeled along-axis velocity profiles compare well with measured profiles (Fig. 4).

In both cases, the outflow and rightward transversal currents were strongest at the northern shore (Fig. 6e, f). This is probably due to gentler slopes and shallower banks along the northern *Petit Lac* shore causing stronger downwind currents in both cases (ESM Fig. S6), and nearshore divergence at the northwestern end of the *Grand Lac* in early winter, which results in a surface depression northeast of the confluence and produces strong barotropic pressure gradients accelerating the outflow in this section of the confluence (ESM Figs. S6, S7, and S8). This highlights the importance of bathymetric effects and spatial heterogeneity and is further discussed in the Momentum budget analysis section below.

Momentum budget analysis

In this section, the processes that produce the observed current patterns at the confluence are investigated by model-based momentum budgets. The temporal development is discussed below by considering the same three phases: initialization, adjust-

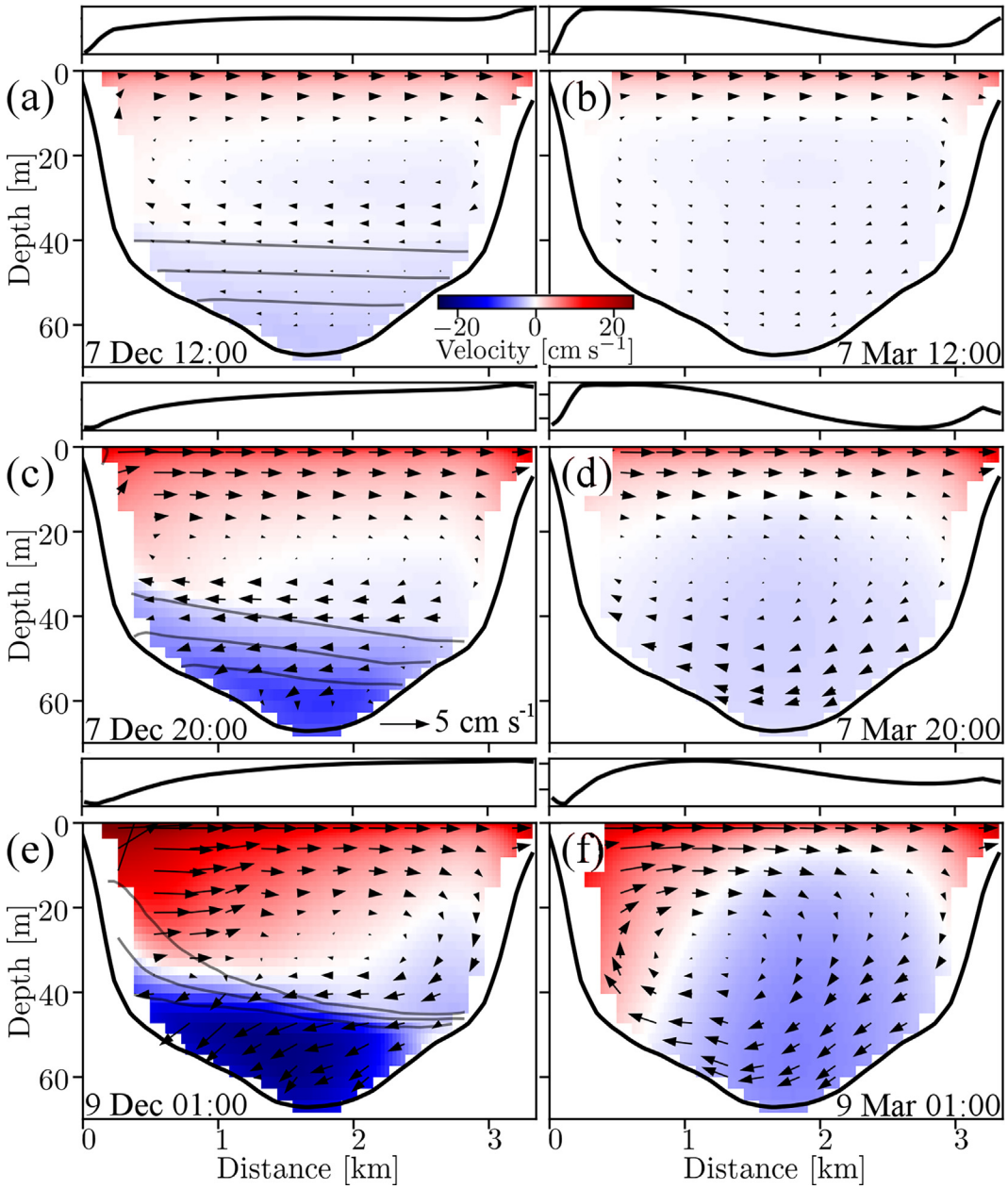

Fig. 6. Modeled current velocities at the confluence in early winter (left column) and late winter (right column), during the initialization (a, b) and adjustment (c, d) phases, and when the circulation was fully developed (e, f). Axial velocities are depicted by color (see colorbar in panels a and b) and transversal velocities by black arrows. The grey contour lines in the left panels mark the 7, 8 and 9 °C isotherms (from bottom to top). Red indicates outflow into the *Grand Lac* and blue, inflow into the *Petit Lac*. The black curve above each 2D transect shows the shape of the corresponding modeled free surface elevation. Distance along the transect is given from the northern shore. The location of the transect and orientation of the axial and transversal directions are shown in Fig. 1a. The transversal velocity scale is given in panel (c). For better visualization, vertical velocities are scaled up by a factor of 20. (For interpretation of the references to color in this figure legend, the reader is referred to the web version of this article.)

ment, and fully-developed circulation. Figs. 8 and 9 show the leading terms (Eq. (1)) in the axial and transversal momentum balances, along a full-depth profile at the confluence center in early (left panels) and late (right panels) winter. Positive terms are directed into the *Grand Lac* in the axial balances and towards the northern shore in the transversal balances (Fig. 1a, red arrows). To allow for a comparison between the governing momentum terms, full-depth profiles at the confluence center, i.e., at the mooring location (Fig. 1a, blue cross), are considered here. The corresponding time-averaged terms at the entire confluence transect are shown in ESM Figs. S8 and S9 for the axial direction.

Initialization phase. Shortly after the wind started, the axial momentum balances in the upper layer were similar in both simulations. Wind stress-induced friction by far dominated, penetrating to a depth of ~30 m (Fig. 8a, b). The positive friction term was partially balanced by a negative barotropic pressure gradient, due to a water level setup induced by downwind surface drift (ESM Fig. S7). The rightward, transversal currents near the surface induced an axial, negative Coriolis acceleration. Its magnitude decreased with depth and changed sign below 20-m depth, i.e., the depth where the transversal currents changed from right- to leftward (Fig. 6a, b). The net axial balance in the upper 15 to 20 m produced a strong acceleration towards the *Grand Lac*.

In the fully-mixed late winter case, all axial terms below 30-m depth were constant, with the balance between the barotropic pressure gradient and the Coriolis acceleration resulting in an acceleration into the *Petit Lac*. Note the constant total pressure gra-

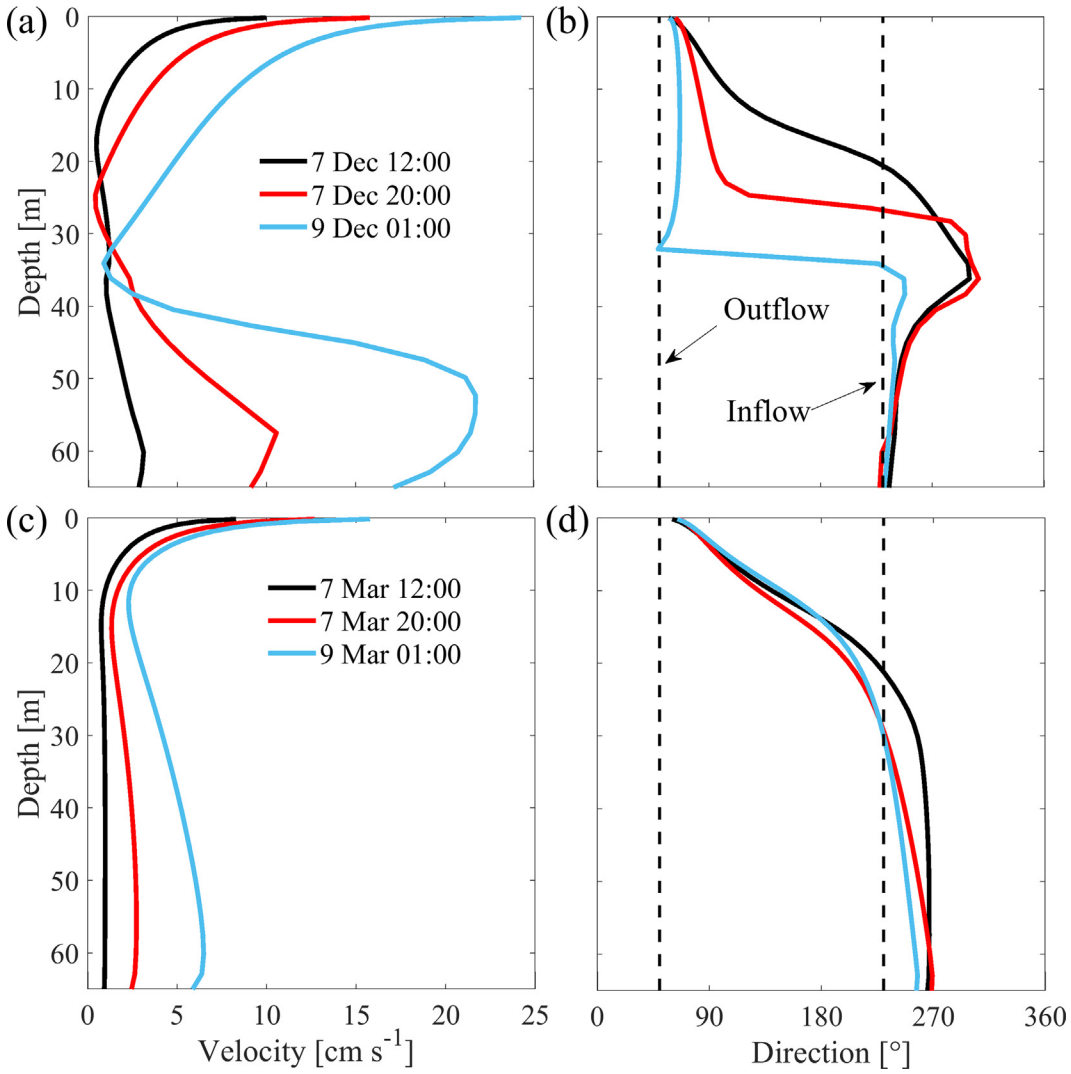

Fig. 7. For early winter (upper panels) and late winter (lower panels): Modeled current velocity (a, c) and direction (b, d) at the confluence center during the initialization (black) and adjustment (red) phases, and when the circulation was fully developed (blue). Dates and times are given in the legend in (a) and (c). The vertical black dashed lines in (b) and (d) mark the outflow and inflow directions, respectively. (For interpretation of the references to color in this figure legend, the reader is referred to the web version of this article.)

dient throughout the water column, thus confirming that baroclinicity was negligible in late winter (Fig. 8b). In contrast, in early winter, negative baroclinic pressure gradients emerged below the thermocline at ~35-m depth, enhancing the inflow near the bottom (Fig. 8a).

Similar to the axial direction, the transversal momentum terms in the upper layers were comparable under both stratification regimes. In the uppermost 10 m, the wind-driven outflow produced a strong, negative Coriolis acceleration, which was largely balanced by positive wind-induced friction, illustrating that the wind stress was not perfectly aligned with the along-axis direction (Fig. 9a, b).

In early winter, there was a geostrophic balance in the transversal direction between the positive Coriolis acceleration below the thermocline due to the inflow, and the baroclinic pressure gradients due to the onset of coastal upwelling (Fig. 9a). In late winter, all transversal terms were small below the wind-affected surface layers, with the barotropic pressure gradient opposing the Coriolis acceleration caused by the weak inflow in the interior.

Adjustment phase. The increasing wind-induced axial friction was partially balanced by the Coriolis and barotropic pressure gradient terms, accelerating the upper layer currents towards the *Grand Lac* (Fig. 8c, d). In fully-mixed late winter, the wind stress almost penetrated down into the entire water column, whereas it was confined to the epilimnion when stratification was present. Since the same wind energy was distributed over a smaller volume, this resulted in overall higher axial frictional forces in the upper layers, explaining the stronger outflow in early winter (Figs. 6 and 7). As a consequence of the stronger outflow, the transversal Coriolis acceleration towards the southern shore was also significantly higher in early winter (Fig. 9c, d). This would imply stronger rightward currents in the upper layers and thus an enhanced transversal secondary circulation. However, as discussed above, the transversal velocities were comparably strong in both cases (Fig. 6c, d), which can be explained by the different signs of the barotropic pressure gradients as detailed below.

In early winter, due to the relatively uniform outflow from the entire epilimnion, Ekman transport towards the southern shore produced an upward tilt of the free surface from left to right (Fig. 6c), resulting in positive transversal barotropic pressure gradients opposing the Coriolis acceleration (Fig. 9c). In late winter, on the other hand, transversal convergence and divergence between the outflow-dominated nearshore regions and inflow-dominated

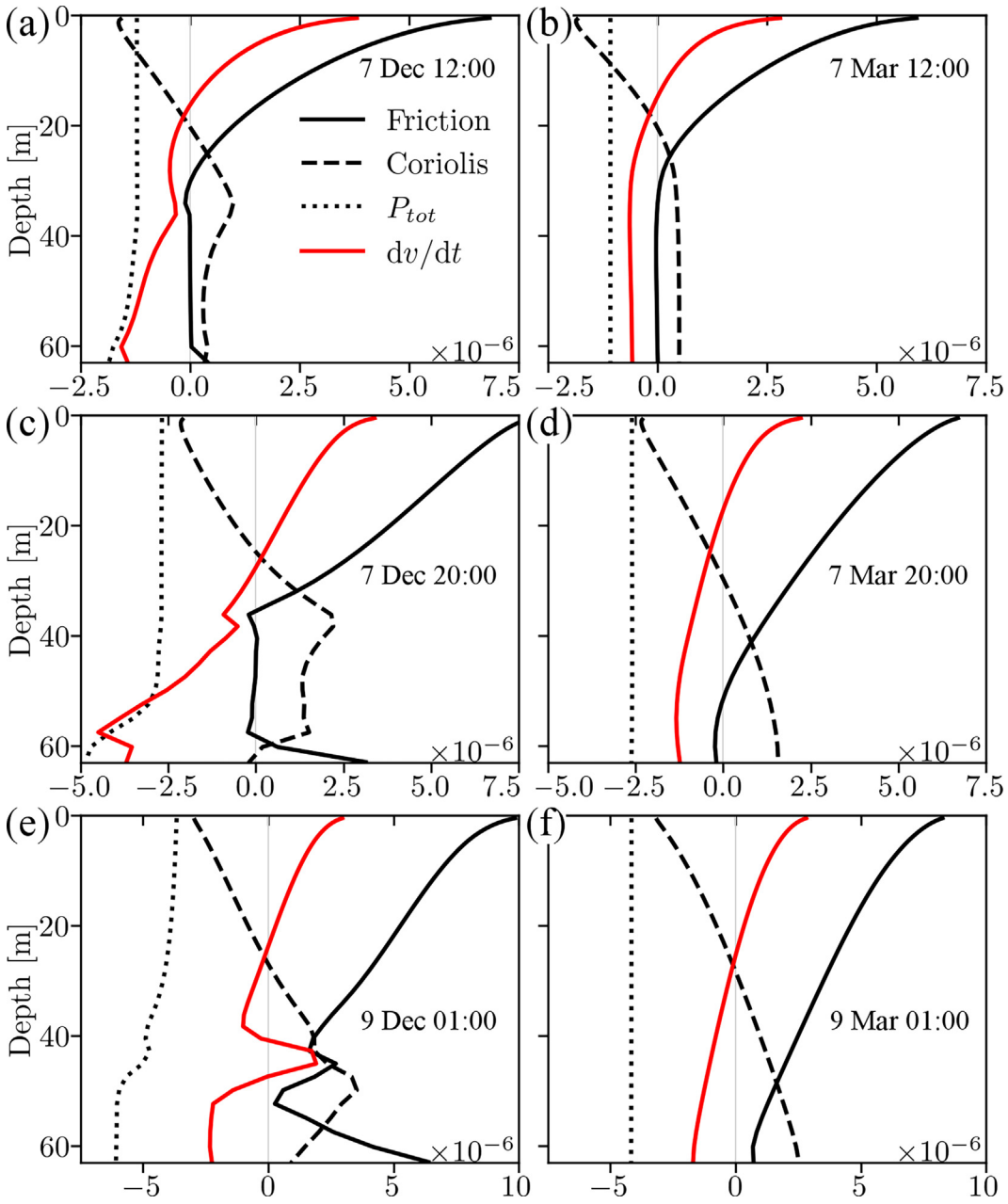

Fig. 8. For early winter (left column) and late winter (right column): Leading terms of the axial momentum balance at the confluence center (blue cross in Fig. 1a) during the initialization (a, b) and adjustment (c, d) phases, and when the circulation was fully developed (e, f). The red curves give the left side of the momentum balance equation, i.e., the local net acceleration, Eq. (1). The unit of the values on the *x*-axis is m s^{-2}. The orientation of the axial axis is shown in Fig. 1a. Lines are defined in panel (a). Date and time are indicated in each panel. For clarity, only the total pressure gradient (barotropic and baroclinic) is shown. (For interpretation of the references to color in this figure legend, the reader is referred to the web version of this article.)

interior produced an undulating free surface (Fig. 6d). This resulted in negative transversal barotropic pressure gradients at the confluence center, acting together with the Coriolis acceleration (Fig. 9d). The opposing signs of the transversal barotropic pressure gradients between early and late winter, acting either with or against the Coriolis acceleration, can explain the observed differences in the vertical structure of the upper currents: During early winter stratification, the net currents gradually approach a more unidirectional structure, whereas they continue to veer strongly with depth during the fully-mixed late winter (Fig. 7b, d, red curves).

In the lower layers, the momentum balances during the adjustment phase showed a continuation of the trends observed during the first hours. In early winter, the negative axial baroclinic pressure gradients near the bottom, caused by upwind upwelling in the *Grand Lac* (Fig. 5a) increased, further strengthening the hypolimnetic inflow. Note that here, baroclinic and barotropic pressure gradients acted in synergy to enhance the hypolimnetic inflow into the shallow basin. This is different from the "classical" situation during upwelling at the upwind end of a basin, where baroclinic (due to upwelling) and barotropic (due to surface setup) pressure gradients oppose each other. The stronger bottom inflow resulted in higher bottom friction (Fig. 8c) and transversal Coriolis acceleration (Fig. 9c), enhancing the coastal upwelling at the northern *Petit Lac* shore while maintaining a geostrophic balance. In late winter, the weak inflow in the interior was driven by barotropic pressure gradients that were balanced by friction and Coriolis terms (Fig. 8d). The transversal terms were qualitatively similar to the initialization phase.

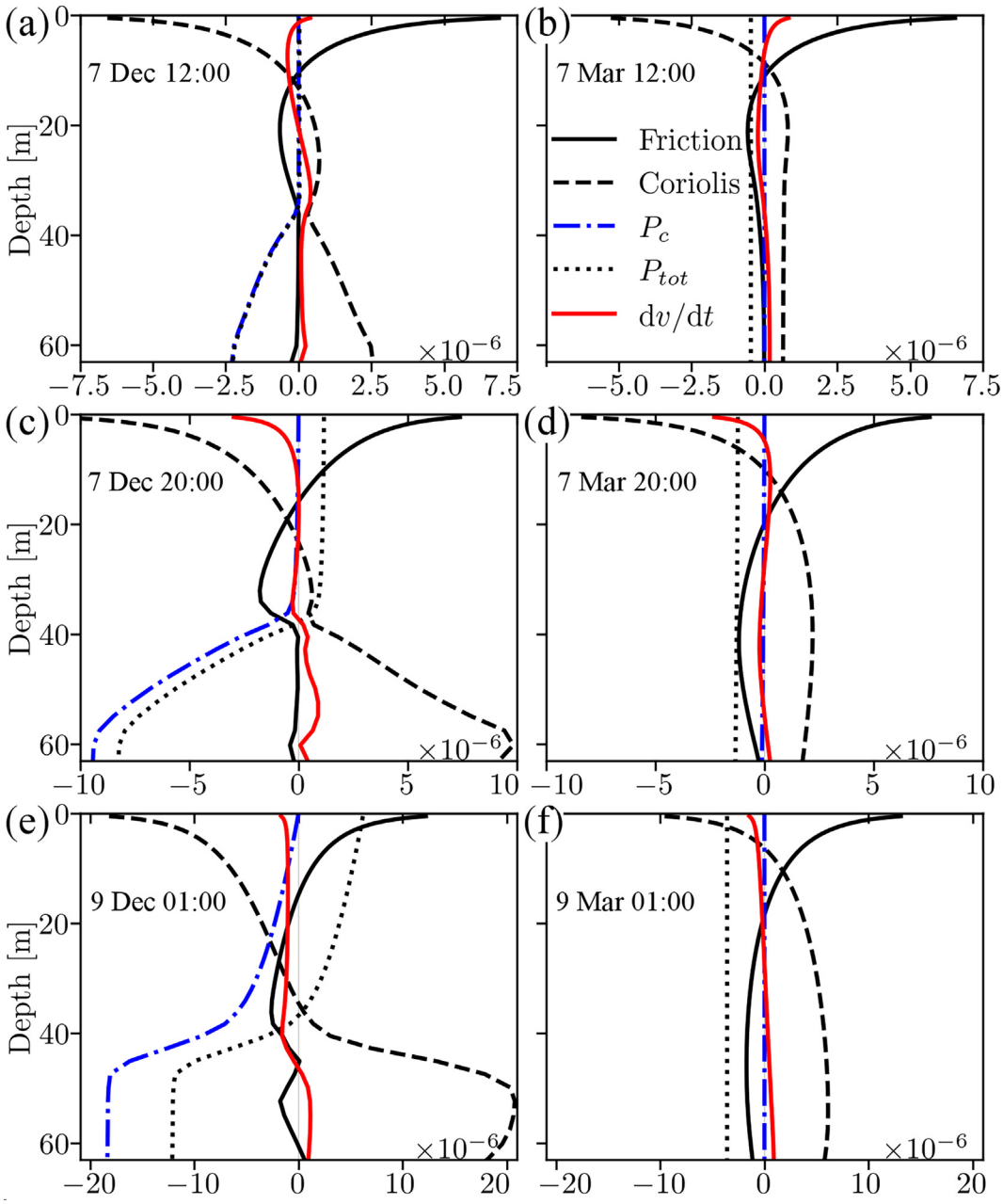

Fig. 9. For early winter (left column) and late winter (right column): Leading terms of the transversal momentum balance at the confluence center (blue cross in Fig. 1a) during the initialization (a, b) and adjustment (c, d) phases, and when the circulation was fully developed (e, f). The red curves give the left side of the momentum balance equation, i.e., the local net acceleration, Eq. (1). The unit of the values on the *x*-axis is m s^{-2}. The orientation of the transversal axis is shown in Fig. 1a. Lines are defined in panel (a). Date and time are indicated in each panel. (For interpretation of the references to color in this figure legend, the reader is referred to the web version of this article.)

Fully-developed circulation. In stratified early winter, axial baroclinicity became more important as wind stress continued, affecting almost the entire water column (Fig. 8e) and illustrating continuous upwind upwelling in the western *Grand Lac*. Furthermore, the thickness of the frictional bottom boundary layer increased. Note the "bump" in the net acceleration between 40 and 50-m depth (Fig. 8e), which was caused by strong advection. This illustrates that nonlinearity could be of leading order in the fully-developed, energetic early winter circulation, especially in the lower layers (see also ESM Fig. S8e). The latter was likely due to the interaction of the strong currents with the local bottom topography (Cimatoribus et al., 2018), which is a known phenomenon in estuarine exchange (e.g., Giddings and MacCready, 2017).

In the upper layers, the stronger axial currents in early winter produced a transversal Coriolis acceleration almost twice as high as in late winter (Fig. 9e, f). However, since it was largely balanced by barotropic pressure gradients caused by the transversal free surface tilt (Fig. 6e), the currents in early winter were unidirectional throughout the epilimnion, whereas they remained depth-veering in late winter (Fig. 7b, d). As a result, the strength of the transversal secondary circulation was similar in both cases (Fig. 6e, f; see also ESM Fig. S5e, f). Note that when stratification was present, the discussed flow adjustment in the upper layers going from initially depth-veering to unidirectional, was also observed in the ADCP measurements (compare Fig. 7a, b and ESM Fig. S10), thus showing the good agreement between the model results and the field observations.

In contrast, in fully-mixed late winter, the axial momentum balance of the fully-developed circulation was characterized by smooth profiles of the frictional and Coriolis terms, approximately linearly

decreasing and increasing from top to bottom, respectively (Fig. 8f). The transversal balance between the Coriolis, barotropic pressure gradient and friction terms resulted in negative accelerations in the upper layers and positive accelerations in the lower layers, in agreement with the transversal clockwise vortex (Figs. 6f and 9f).

The fully-developed axial circulation in late winter resembled the wind-driven circulation in a non-rotating, elongated, non-stratified basin with sloping boundaries, as discussed, for example, by Winant (2004) and Sanay and Valle-Levinson (2005). This circulation is characterized by intense downwind flow over the shallow banks and near the surface, balanced by upwind flow in the interior. In a rotating basin deeper than one Ekman depth, the axial circulation is similar, but with reduced magnitude, while a transversal clockwise vortex (when looking downwind) develops that spans the cross-section (e.g., Ponte et al., 2012; Sanay and Valle-Levinson, 2005; Winant, 2004). Here, the Ekman depth is a measure relating the frictional force to the Coriolis force and is defined as $d_E = \sqrt{2K_v/f}$, where f is the latitude-dependent Coriolis parameter, O (10^{-4} s^{-1}), and K_v is the vertical eddy viscosity (e.g., Amadori et al., 2020). In the model employed in the present study, K_v is computed by the K-Profile Parameterization (KPP; Large et al., 1994) and can be output from MITgcm as a diagnostic term. Taking a typical value of $K_v = 300$ cm^2, s^{-1} during the late winter wind event as the cross-sectional average at the confluence 1.5 d after the wind started (Sanay and Valle-Levinson, 2005), one obtains $d_E \approx 15$ m.

Considering a typical Ekman depth smaller than the maximum confluence depth of 65 m, the elongated shape of the *Petit Lac*, and the spatially fairly homogeneous, steady *Vent* wind, the late winter case studied here is comparable to those described in the literature cited above, thus explaining the general circulation patterns (Fig. 6f). For a uniform wind acting on a symmetric basin and ignoring nonlinear effects, the resulting axial circulation is symmetrical with respect to the cross-section center (Winant, 2004). However, Ponte et al. (2012) showed that the core of the upwind interior flow could shift towards the shores when nonlinear effects are included and a spatially varying wind field is imposed. This results in a slanted, inverse-U-shaped zero-isotach, similar to the pattern observed here. In our case, the stronger downwind currents at the northern shore of the *Petit Lac*, caused by the gentler slopes and shallower banks, are probably the reason for the observed asymmetries (Fig. 6f and ESM Fig. S6). An undulating free surface at the confluence (Fig. 6, right panels) was also reported by Sanay and Valle-Levinson (2005) when considering a rotating basin. A similar wind-driven transversal (secondary) circulation in an elongated basin under the effect of rotation was observed in the deep and narrow northern basin of Lake Garda, Italy (max. depth 350 m, width ~2–4 km), where it was associated with deep-water ventilation (Piccolroaz et al., 2019).

Effect of stratification on wind-driven interbasin exchange

Strength of interbasin exchange

The differences in the circulation patterns between the stratified early winter and fully-mixed late winter cases discussed above have important consequences for the wind-induced interbasin exchange in Lake Geneva. The volume exchange across the confluence transect was estimated by integrating the modeled inflowing (or outflowing) velocities in time and space (Fig. 6, blue and red areas, respectively). When considering the 2.5-d wind period, the accumulated volume transport into the *Petit Lac* was

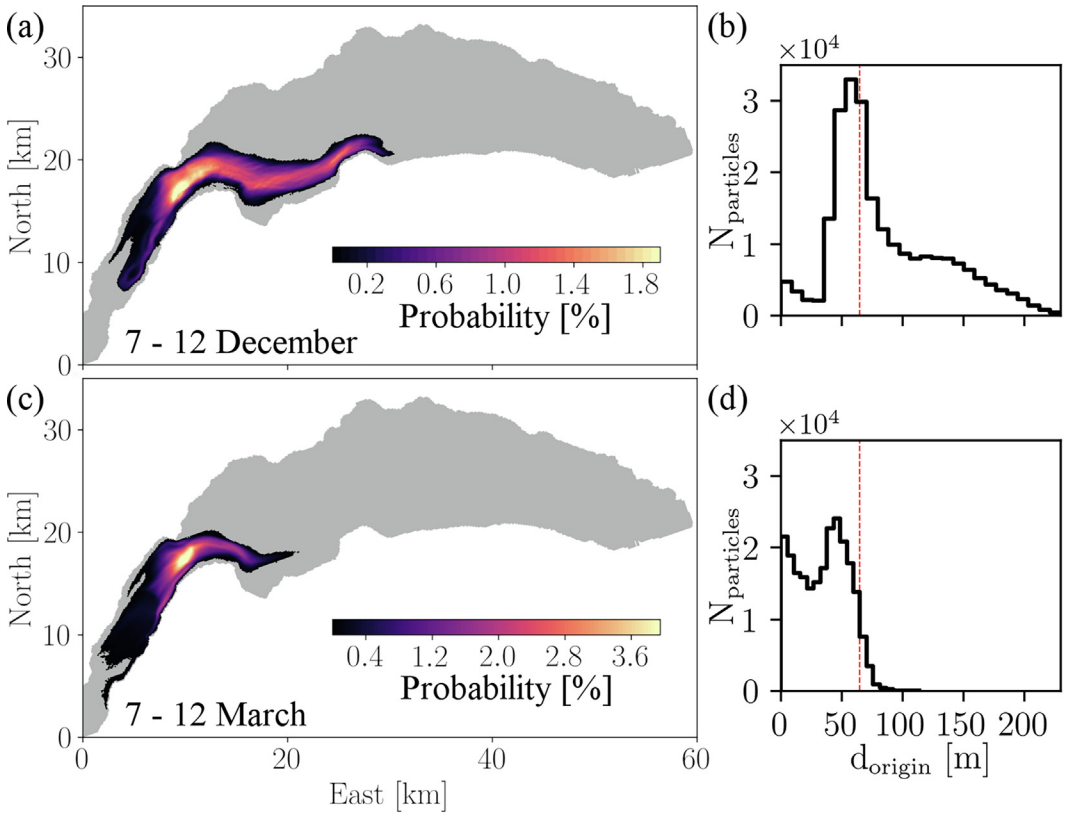

Fig. 10. Probability maps derived from the backward particle tracking simulations showing dominant particle pathways during the early (a) and late (c) winter cases. Particles were released in the *Petit Lac*; release area shown in ESM Fig. S1. Histograms of the particle origin depths during early (b) and late (d) winter. The red dashed lines in (b) and (d) mark the maximum depth of the confluence (65 m). Probabilities are shown by colorbars and reflect the total number of different particles that visited each 113 m × 113 m model grid cell during the entire simulation, divided by the total number of particles. For clarity, cells with less than 50 particles are not shown. (For interpretation of the references to color in this figure legend, the reader is referred to the web version of this article.)

$Q_{in,early} \approx 0.88$ km^3 during early winter and $Q_{in,late} \approx 0.46$ km^3 during late winter. Furthermore, driven by the baroclinic pressure gradients at the confluence (due to upwind upwelling in the wider, deeper basin), the bottom inflow in early winter continued for ~1.5 d after the wind ceased, maintaining velocities of ~10 cm s^{-1} (also seen in the field observations, ESM Fig. S4). In late winter, on the other hand, the inflow rapidly stopped after the wind ceased. Considering this enhanced inflow caused by the baroclinicity, we obtain $Q_{in,early} \approx 1.64$ km^3 and $Q_{in,late} \approx 0.71$ km^3. This illustrates that during a single early-winter *Vent* event, more than half of the total *Petit Lac* volume (~3 km^3) was exchanged across the confluence into the *Grand Lac* basin. Such an enhanced flushing can be of great ecological interest, for example, if the shallow basin is subject to significant loads of nutrients and/or contaminants (e.g., Kempenfelt Bay in Lake Simcoe; Flood et al., 2020). In late winter, however, the accumulated interbasin exchange was reduced by a factor of ~2.3, due to the weaker and depth-veering currents. In summary, under identical wind forcing, the flushing of the *Petit Lac* basin was less than 50 % as efficient in late winter when no stratification was present.

Horizontal and vertical exchange patterns and hypolimnetic upwelling

The origin of the deep *Petit Lac* waters was determined by backward tracking of particles released in its bottom layers during the first days of the wind event. Fig. 10 shows histograms of the particle origin depth, as well as dominant pathways taken by the particles in the form of probability maps (e.g., van Sebille et al., 2018).

In early winter, more than half of the particles originated from below 65-m depth, the maximum depth at the confluence, with a significant number coming from depths between 100 and 200 m (Fig. 10b), thus confirming the upwelling of deep, hypolimnetic *Grand Lac* water into the shallow basin as indicated by the observed bottom temperatures (Fig. 3c). Furthermore, the upwelled particles had already traveled up to 20 km in the *Grand Lac* before entering the *Petit Lac*, showing that large areas of the deep hypolimnion were affected by these vertical and horizontal exchange processes (Fig. 10a). Once upwelled, strong bottom currents (Fig. 6c, e) transported these waters far into the shallow basin, before they finally descended back into the deeper basin a few days after the wind had ceased. This is discussed in detail by Reiss et al. (2022), who showed that *Vent* winds regularly generate a "current loop" in weakly stratified Lake Geneva, whereby deep, hypolimnetic *Grand Lac* waters first upwell into the *Petit Lac*, are then transported more than 10 km into the *Petit Lac* basin, before ultimately descending back into the hypolimnion of the *Grand Lac*.

Due to the mild climate and its great depth (309 m), the *Grand Lac* basin remains stratified during most seasons, with complete convective overturning only occurring occasionally during severely cold winters. As a result, lower DO and higher nutrient concentrations are found in the deep hypolimnion compared to the shallow *Petit Lac* basin (e.g., CIPEL, 2019). Wind-driven upwelling between the two basins during stratified early winter could therefore provide a potentially important mechanism for vertical exchange and deepwater renewal in Lake Geneva, similar to what has been observed in Lake Erie (e.g., Bartish, 1987).

In contrast, in late winter only 5 % of the particles originated from below 65-m depth in the *Grand Lac*, with virtually none coming from below the thermocline (Fig. 10d). This confirms that the upwind upwelling in the *Grand Lac* did not extend into the *Petit Lac* (Fig. 5b), which agrees with the measurements taken during a comparable *Vent* event in March 2019, when constant near-bottom temperatures were observed at the confluence (Fig. 3). Overall, in late winter no upwelling of deep, hypolimnetic waters from the *Grand Lac* into the shallow *Petit Lac* occurred and the exchange between the basins was more horizontal, which can be explained by the baroclinically decoupled basins. Furthermore, the bulk of the particles that were drawn from the *Grand Lac* into the *Petit Lac* originated from the immediate vicinity of the confluence with only the waters near the confluence being affected, thus illustrating that the exchange was more local than in early winter (Fig. 10c). This is due to the overall weaker currents and the depth-veering structure of the outflow (Fig. 7). These results demonstrate that in the unstratified case, wind-driven interbasin exchange has less impact on the basin-wide transport and potentially on its ecology.

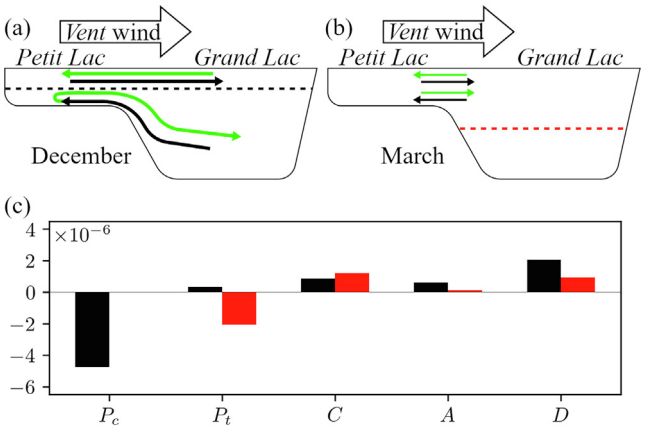

Fig. 11. Summary of wind-induced interbasin exchange processes between the *Petit Lac* and *Grand Lac* of Lake Geneva. Current patterns for (a) early winter, weakly stratified (December) and (b) late winter, fully-mixed (March) conditions. Cross-sections are vertically exaggerated. Horizontal black and red dashed lines: thermocline depths. Black arrows: currents during the fully-developed circulation. Green arrows: relaxation flows after the wind ceased. Arrow thickness: intensity of the exchange flow (~50 % smaller in late winter than in early winter). Arrow length: approximate distance traveled by exchange flows. Note that deep upwelling from the *Grand Lac* hypolimnion into the *Petit Lac* basin only occurs in the early winter (a). These cold waters then drain back into the *Grand Lac* hypolimnion after the *Vent* wind has ceased, thus forming a current "loop" which contributes to deepwater renewal. (c) Mean terms of the axial momentum balance (in m s^{-2}; see Eq. (1) for details) in early (black) and late (red) winter, depth-averaged below 35-m depth and averaged over the entire *Vent* wind event. Horizontal axis: P_c baroclinic pressure gradient term, P_t barotropic pressure gradient term, C Coriolis acceleration, A nonlinear advection term, and D dissipation due to bulk and bottom friction. (For interpretation of the references to color in this figure legend, the reader is referred to the web version of this article.)

The main effect of stratification and Coriolis force on the exchange between the two basins of Lake Geneva during winter are schematically summarized in Fig. 11. Significant differences exist between the circulation during weakly stratified early winter (December; Fig. 11a) and fully-mixed late winter (March; Fig. 11b). From the axial momentum balance averaged over the whole *Vent* event, it is evident (Fig. 11c) that during weak stratification, baroclinicity is the driver of the deepwater upwelling of cold hypolimnic waters from the *Grand Lac* basin into the *Petit Lac*. Upwelling does not occur when the *Petit Lac* is fully-mixed.

Summary and conclusions

Combining field observations, three-dimensional (3D) hydrodynamic modeling, and particle tracking, we demonstrated the significant effect that stratification can have on wind-driven interbasin exchange between the shallow basin and the deep basin of a large lake during winter. Current and temperature profiles taken at the confluence between the shallow *Petit Lac* (maximum depth 75 m) and deep *Grand Lac* (maximum depth 309 m) basins of Lake Geneva showed markedly different patterns during two comparably strong, typical along-axis *Vent* wind events (from the southwest) in December 2018 (early winter) when the *Petit Lac* was weakly stratified with a thermocline at ~35-m depth, and in March 2019

(late winter) when it was fully-mixed. To quantify the effect of stratification on the exchange process between the two lake basins, we carried out two 3D simulations with identical external forcing, but different stratification, representing typical early and late winter conditions. The observed early/late winter differences were well reproduced by the numerical model, which allowed us to investigate and quantify for the first time in a lake, the driving mechanisms behind the two circulation patterns by means of a momentum budget analysis.

The key features, similarities and differences in the interbasin exchange dynamics between the *Grand Lac* and the weakly stratified (early winter) or fully-mixed (late winter) shallow *Petit Lac* can be summarized as follows (see also schematic summary in Fig. 11):

- For both stratification regimes, the *Vent* wind from the southwest produces "upwind upwelling" at the western end of the *Grand Lac* basin, near the confluence. This is due to horizontal current divergence caused by the different widths of the basins.
- In early winter, a two-layer flow is established with the downwind epilimnetic currents flowing towards the *Grand Lac* (outflow) balanced by hypolimnetic countercurrents flowing into the *Petit Lac* (inflow). The rightward Ekman transport in the epilimnion produces an upward tilt of the free surface towards the southern *Petit Lac* shore. This generates barotropic pressure gradients that largely balance the Coriolis acceleration due to the epilimnetic outflow, resulting in unidirectional currents aligned with the wind.
- In early winter, the upwind upwelling in the *Grand Lac* produces axial baroclinic pressure gradients at the confluence that are the main driver for the strong bottom inflow into the *Petit Lac* and significantly enhance interbasin exchange by strengthening the currents and causing the bottom inflow into the *Petit Lac* to persist for more than one day after the wind ceased.
- In early winter, deep hypolimnetic *Grand Lac* waters, originating from more than 20 km away, upwell into the *Petit Lac*. These upwelled waters then travel far into the shallow basin, before ultimately (after the wind has ceased) returning back into the deep *Grand Lac*. This current "loop" provides a potential ecologically important mechanism not only for horizontal, but also vertical exchange, and thus, deepwater renewal.
- In late winter, with the thermocline well below the *Petit Lac* depth, the upwind upwelling at the western *Grand Lac* does not reach the bottom of the confluence. Therefore, interbasin exchange and the circulation in the *Petit Lac* are purely wind-driven and baroclinicity no longer plays a role (Fig. 11c). Consequently, exchange currents are considerably weaker and the net volume exchange between the basins is reduced by more than a factor of two compared to the stratified early winter case.
- In late winter, interbasin exchange is more local, affecting only the *Grand Lac* waters in close proximity to the confluence, and is mainly horizontal; thus, no upwelling of hypolimnetic *Grand Lac* waters into the shallow basin occurs.
- The late winter circulation in the *Petit Lac* resembles that of a steady, wind-driven circulation in a rotating, fully-mixed, elongated basin with sloping boundaries and a depth greater than one Ekman depth. This circulation is characterized by downwind flow over the shallow nearshore regions and near the surface, and upwind flow in the intermediate layers. Due to the Coriolis force, a clockwise rotating vortex with a horizontal axis (when looking downwind) develops in the transversal plane, and the upper-layer currents in the interior veer to the right with depth.

Global warming is expected to continue weakening wintertime convective cooling in Lake Geneva. This will result in less frequent complete overturning and longer stratification periods, which have already been recorded globally in lakes (Arvola et al., 2010; Woolway et al., 2020). Therefore, the probability of deepwater renewal by convective cooling will decrease. On the other hand, based on our findings, a prolonged winter stratification of the shallow *Petit Lac* basin will also extend the period during which wind-induced interbasin exchange can produce strong upwelling of deep hypolimnetic *Grand Lac* waters (cf. Reiss et al., 2022 for further details). As a consequence, wind-induced interbasin upwelling will become an increasingly more important process for vertical exchange and deepwater renewal in the *Grand Lac* basin under current climate change scenarios. At present, *Vent* winds are the most frequent strong winter winds in the region and are projected to remain strong (e.g., CH2018, 2018). No systematic wind stilling over Switzerland and no significant changes in near-surface mean wind speed are expected until the end of the 21st century (Graf et al., 2019), suggesting that wind-induced interbasin upwelling and subsequent deepwater renewal in the *Grand Lac* basin will remain strong in the future.

The findings of this study have advanced the understanding of multi basin wintertime dynamics in large lakes, which is presently lacking. It was demonstrated that wind-induced interbasin exchange in Lake Geneva in winter is a complex 3D process that is strongly affected by the Coriolis force and stratification. The discussed underlying mechanisms, processes and driving forces, and their interactions in controlling interbasin exchange dynamics are not lake-specific. Therefore, these processes can be expected to play a key role in the interbasin exchange in other large multi-basin lakes under similar conditions. They should be considered when developing long-term lake management concepts, in particular with respect to deepwater renewal.

Declaration of Competing Interest

The authors declare that they have no known competing financial interests or personal relationships that could have appeared to influence the work reported in this paper.

Acknowledgments and data availability

This work was supported by the Swiss National Science Foundation (SNSF grant no. 159422) and the Bois Chamblard Foundation (last accessed on 28 October 2022). Meteorological data were provided by the Federal Office of Meteorology and Climatology in Switzerland (MeteoSwiss, last accessed on 28 October 2022). Full-depth temperature profile data at SHL2 were provided by © OLA-IS, AnaEE-France, INRAE of Thonon-les-Bains, CIPEL (Rimet et al., 2020). We thank Htet Kyi Wynn and Benjamin Graf for assisting with the fieldwork.

Appendix A. Supplementary data

Supplementary data to this article can be found online at https://doi.org/10.1016/j.jglr.2023.02.005.

References

Ahrnsbrak, W.F., Wing, M.R., 1998. Wind-induced hypolimnion exchange in Lake Ontario's Kingston basin: Potential effects on oxygen. J. Great Lakes Res. 24, 145–151. https://doi.org/10.1016/S0380-1330(98)70806-8.

Amadori, M., Piccolroaz, S., Dijkstra, H.A., Toffolon, M., 2020. What makes an elongated lake 'large'? Scales from wind-driven steady circulation on a rotating Earth. J. Great Lakes Res. 46, 703–717. https://doi.org/10.1016/j.jglr.2019.10.013.

Anderson, E.J., Schwab, D.J., 2013. Predicting the oscillating bi-directional exchange flow in the Straits of Mackinac. J. Great Lakes Res. 39, 663–671. https://doi.org/10.1016/j.jglr.2013.09.001.

Anderson, E.J., Schwab, D.J., 2017. Meteorological influence on summertime baroclinic exchange in the Straits of Mackinac. J. Geophys. Res. Oceans 122, 2171–2182. https://doi.org/10.1002/2016JC012255.

Appt, J., Imberger, J., Kobus, H., 2004. Basin-scale motion in stratified Upper Lake Constance. Limnol. Oceanogr. 49, 919–933. https://doi.org/10.4319/lo.2004.49.4.0919.

Arvola, L., George, G., Livingstone, D.M., Järvinen, M., Blenckner, T., Dokulil, M.T., Jennings, E., Aonghusa, C.N., Nõges, P., Nõges, T., Weyhenmeyer, G.A., 2010. The impact of the changing climate on the thermal characteristics of lakes. In: George, G. (Ed.), The Impact of Climate Change on European Lakes. Aquatic Ecology Series, vol. 4. Springer, Dordrecht, pp. 85–101. https://doi.org/10.1007/978-90-481-2945-4_6.

Bartish, T., 1987. A review of exchange processes among the three basins of Lake Erie. J. Great Lakes Res. 13, 607–618. https://doi.org/10.1016/S0380-1330(87)71676-1.

Boyce, F.M., Chiocchio, F., Eid, B., Penicka, F., Rosa, F., 1980. Hypolimnion flow between the central and eastern basins of Lake Erie during 1977 (Interbasin hypolimnion flows). J. Great Lakes Res. 6, 290–306. https://doi.org/10.1016/S0380-1330(80)72110-X.

Brett, G.J., Pratt, L.J., Rypina, I.I., Sánchez-Garrido, J.C., 2020. The Western Alboran Gyre: An analysis of its properties and its exchange with surrounding water. J. Phys. Oceanogr. 50, 3379–3402. https://doi.org/10.1175/JPO-D-20-0028.1.

CH2018, 2018. Climate Scenarios for Switzerland, Technical Report, National Centre for Climate Services, Zurich, 271 pp. ISBN: 978-3-9525031-4-0. Retrieved from https://naturalsciences.ch/service/publications/107865-ch2018—climate-scenarios-for-switzerland-technical-report, last accessed 28 October 2022.

Cimatoribus, A.A., Lemmin, U., Bouffard, D., Barry, D.A., 2018. Nonlinear dynamics of the nearshore boundary layer of a large lake (Lake Geneva). J. Geophys. Res. Oceans 123, 1016–1031. https://doi.org/10.1002/2017JC013531.

Cimatoribus, A.A., Lemmin, U., Barry, D.A., 2019. Tracking Lagrangian transport in Lake Geneva: A 3D numerical modeling investigation. Limnol. Oceanogr. 64, 1–18. https://doi.org/10.1002/lno.11111.

Cimatoribus, A.A., 2018. C-tracker. doi:10.5281/zenodo.1034118

CIPEL, 2016. Rapports sur les études et recherches entreprises dans le bassin lémanique, Campagne 2015. Commission internationale pour la protection des eaux du Léman (CIPEL), Nyon, Switzerland. Retrieved from https://www.cipel.org/wp-content/uploads/2021/06/rapportscientifique-camp-2015-vf.pdf, last accessed 28 October 2022.

CIPEL, 2019. Rapports sur les études et recherches entreprises dans le bassin lémanique, Campagne 2018. Commission internationale pour la protection des eaux du Léman (CIPEL), Nyon, Switzerland. Retrieved from https://www.cipel.org/wp-content/uploads/2021/06/rapportscientifique-camp-2018-vf.pdf, last accessed 28 October 2022.

Döös, K., Kjellsson, J., Jönsson, B., 2013. TRACMASS—A Lagrangian trajectory model. In: Soomere, T., Quak, E. (Eds.), Preventive Methods for Coastal Protection: Towards the Use of Ocean Dynamics for Pollution Control. Springer, Heidelberg, pp. 225–249. https://www.springerprofessional.de/en/tracmass-a-lagrangian-trajectory-model/1994902, last accessed 28 October 2022.

Flood, B., Wells, M., Dunlop, E., Young, J., 2020. Internal waves pump waters in and out of a deep coastal embayment of a large lake. Limnol. Oceanogr. 65, 205–223. https://doi.org/10.1002/lno.11292.

Foroughan, M., Hamze-Ziabari, S.M., Lemmin, U., Barry, D.A., 2022. A persistent submesoscale frontal slick: A novel marker of the mesoscale flow field in a large lake (Lake Geneva) e2022GL100262 Geophys. Res. Lett. 49. https://doi.org/10.1029/2022GL100262.

Giddings, S.N., MacCready, P., 2017. Reverse estuarine circulation due to local and remote wind forcing, enhanced by the presence of along-coast estuaries. J. Geophys. Res. Oceans 122, 10184–10205. https://doi.org/10.1002/2016JC012479.

Graf, W.H., Prost, J.P., 1980. Aerodynamic drag and its relation to the sea state: With data from Lake GenevaAerodynamische Reibung und deren Beziehung zum Seegang; Experimente vom GenferseeLa trainée aérodynamique en relation avec l'état de surface du lac (Le Léman). Arch. Met. Geoph. Biokl. A 29 (1-2), 67–87. https://doi.org/10.1007/BF02247734.

Graf, M., Scherrer, S.C., Schwierz, C., Begert, M., Martius, O., Raible, C.C., Brönnimann, S., 2019. Near-surface mean wind in Switzerland: Climatology, climate model evaluation and future scenarios. Int. J. Climatol. 39, 4798–4810. https://doi.org/10.1002/joc.6108.

Hamblin, P.F., 1998. Exchange flows in Lakes. In: Imberger, J. (Ed.), Physical Processes in Lakes and Oceans. American Geophysical Union, pp. 187–198. https://doi.org/10.1029/CE054p0187.

Hamidi, S.A., Bravo, H.R., Klump, J.V., Waples, J.T., 2015. The role of circulation and heat fluxes in the formation of stratification leading to hypoxia in Green Bay, Lake Michigan. J. Great Lakes Res. 41, 1024–1036. https://doi.org/10.1016/j.jglr.2015.08.007.

Hamze-Ziabari, S.M., Razmi, A.M., Lemmin, U., Barry, D.A., 2022. Detecting submesoscale cold filaments in a basin-scale gyre in large, deep Lake Geneva (Switzerland/France) e2021GL096185 Geophys. Res. Lett. 49. https://doi.org/10.1029/2021GL096185.

Hogg, A.M., Ivey, G.N., Winters, K.B., 2001. Hydraulics and mixing in controlled exchange flows. J. Geophys. Res. Oceans 106, 959–972. https://doi.org/10.1029/2000JC000266.

Imam, Y.E., Laval, B.E., Lawrence, G.A., 2013. The baroclinic response to wind in a small two-basin lake. Aquat. Sci. 75, 213–233. https://doi.org/10.1007/s00027-012-0268-1.

Jabbari, A., Ackerman, J.D., Boegman, L., Zhao, Y., 2019. Episodic hypoxia in the western basin of Lake Erie. Limnol. Oceanogr. 64, 2220–2236. https://doi.org/10.1002/lno.11180.

Jabbari, A., Ackerman, J.D., Boegman, L., Zhao, Y., 2021. Increases in Great Lake winds and extreme events facilitate interbasin coupling and reduce water quality in Lake Erie. Sci. Rep. 11, 5733. https://doi.org/10.1038/s41598-021-84961-9.

Large, W.G., McWilliams, J.C., Doney, S.C., 1994. Oceanic vertical mixing: A review and a model with a nonlocal boundary layer parameterization. Rev. Geophys. 32, 363–403. https://doi.org/10.1029/94RG01872.

Laval, B.E., Morrison, J., Potts, D.J., Carmack, E.C., Vagle, S., James, C., McLaughlin, F. A., Foreman, M., 2008. Wind-driven summertime upwelling in a fjord-type lake and its impact on downstream river conditions: Quesnel Lake and River, British Columbia, Canada. J. Great Lakes Res. 34, 189–203. https://doi.org/10.3394/0380-1330(2008)34[189:WSUIAF]2.0.CO;2.

Lavigne, S., Nirel, P., 2016. Physico-chemical and biological changes in the waters of the Petit Lac. Service de l'écologie de l'eau (SECOE). Geneva, Switzerland. Retrieved from https://www.cipel.org/wp-content/uploads/catalogue/0-evolution-physico-chimique-biologique-petit-lac-camp-2015.pdf, last accessed 28 October 2022.

Lawrence, G., Pieters, R., Zaremba, L., Tedford, T., Gu, L., Greco, S., Hamblin, P., 2004. Summer exchange between Hamilton Harbour and Lake Ontario. Deep-Sea Res. II 51, 475–487. https://doi.org/10.1016/j.dsr2.2003.09.002.

Lemmin, U., Amouroux, A., 2013. The influence of climate change on Lake Geneva. In: Goldman, C.R., Kumagai, M., Robarts, R.D. (Eds.), Climatic Change and Global Warming of Inland Waters: Impacts and Mitigation for Ecosystems and Societies. Wiley-Blackwell, Chichester UK, pp. 201–217. https://doi.org/10.1002/9781118470596.ch12.

Lemmin, U., D'Adamo, N., 1996. Summertime winds and direct cyclonic circulation: Observations from Lake Geneva. Ann. Geophys. 14, 1207–1220. https://doi.org/10.1007/s00585-996-1207-z.

Liu, Q., Anderson, E.J., Zhang, Y., Weinke, A.D., Knapp, K.L., Biddanda, B.A., 2018. Modeling reveals the role of coastal upwelling and hydrologic inputs on biologically distinct water exchanges in a Great Lakes estuary. Estuar. Coast. Shelf Sci. 209, 41–55. https://doi.org/10.1016/j.ecss.2018.05.014.

Marshall, J., Adcroft, A., Hill, C., Perelman, L., Heisey, C., 1997. A finite-volume, incompressible Navier Stokes model for studies of the ocean on parallel computers. J. Geophys. Res. Oceans 102, 5753–5766. https://doi.org/10.1029/96JC02775.

Mesman, J.P., Stelzer, J.A.A., Dakos, V., Goyette, S., Jones, I.D., Kasparian, J., McGinnis, D.F., Ibelings, B.W., 2021. The role of internal feedbacks in shifting deep lake mixing regimes under a warming climate. Freshw. Biol. 66, 1021–1035. https://doi.org/10.1111/fwb.13704.

Niu, Q., Xia, M., Rutherford, E.S., Mason, D.M., Anderson, E.J., Schwab, D.J., 2015. Investigation of interbasin exchange and interannual variability in Lake Erie using an unstructured-grid hydrodynamic model. J. Geophys. Res. Oceans 120, 2212–2232. https://doi.org/10.1002/2014JC010457.

Perroud, M., Goyette, S., 2012. Interfacing a one-dimensional lake model with a single-column atmospheric model: 2. Thermal response of the deep Lake Geneva, Switzerland under a 2 × CO_2 global climate change. Water Resour. Res. 48, W06522. https://doi.org/10.1029/2011WR011222.

Piccolroaz, S., Amadori, M., Toffolon, M., Dijkstra, H.A., 2019. Importance of planetary rotation for ventilation processes in deep elongated lakes: Evidence from Lake Garda (Italy). Sci. Rep. 9, 8290. https://doi.org/10.1038/s41598-019-44730-1.

Ponte, A.L., Gutiérrez de Velasco, G., Valle-Levinson, A., Winters, K.B., Winant, C.D., 2012. Wind-driven subinertial circulation inside a semienclosed bay in the Gulf of California. J. Phys. Oceanogr. 42, 940–955. https://doi.org/10.1175/JPO-D-11-0103.1.

Reiss, R.S., Lemmin, U., Cimatoribus, A.A., Barry, D.A., 2020. Wintertime coastal upwelling in Lake Geneva: An efficient transport process for deepwater renewal in a large, deep lake e2020JC016095 J. Geophys. Res. Oceans 125. https://doi.org/10.1029/2020JC016095.

Reiss, R.S., Lemmin, U., Barry, D.A., 2022. Wind-induced hypolimnetic upwelling between the multi-depth basins of Lake Geneva during winter: An overlooked deepwater renewal mechanism? e2021JC018023 J Geophys. Res. Oceans 127. https://doi.org/10.1029/2021JC018023.

Rimet, F., Anneville, O., Barbet, D., Chardon, C., Crépin, L., Domaizon, I., Dorioz, J.-M., Espinat, L., Frossard, V., Guillard, J., Goulon, C., Hamelet, V., Hustache, J.-C., Jacquet, S., Lainé, L., Montuelle, B., Perney, P., Quetin, P., Rasconi, S., Schellenberger, A., Tran-Khac, V., Monet, G., 2020. The Observatory on LAkes (OLA) database: Sixty years of environmental data accessible to the public: The Observatory on LAkes (OLA) database. J. Limnol. 79, 164–178. https://doi.org/10.4081/jlimnol.2020.1944.

Roberts, D.C., Sprague, H.M., Forrest, A.L., Sornborger, A.T., Schladow, S.G., 2019. Observations and modeling of the surface seiches of Lake Tahoe, USA. Aquat. Sci. 81, 46. https://doi.org/10.1007/s00027-019-0644-1.

Rueda, F.J., Cowen, E.A., 2005. Exchange between a freshwater embayment and a large lake through a long, shallow channel. Limnol. Oceanogr. 50, 169–183. https://doi.org/10.4319/lo.2005.50.1.0169.

Rueda, F.J., Schladow, S.G., Clark, J.F., 2008. Mechanisms of contaminant transport in a multi-basin lake. Ecol. Appl. 18, A72–A88. https://doi.org/10.1890/06-1617.1.

Salmaso, N., 2005. Effects of climatic fluctuations and vertical mixing on the interannual trophic variability of Lake Garda, Italy. Limnol. Oceanogr. 50, 553–565. https://doi.org/10.4319/lo.2005.50.2.0553.

Sanay, R., Valle-Levinson, A., 2005. Wind-induced circulation in semienclosed homogeneous, rotating basins. J. Phys. Oceanogr. 35, 2520–2531. https://doi.org/10.1175/JPO2831.1.

Schertzer, W.M., Assel, R.A., Beletsky, D., Croley, T.E., Lofgren, B.M., Saylor, J.H., Schwab, D.J., 2008. Lake Huron climatology, inter-lake exchange and mean circulation. Aquat. Ecosyst. Health Manag. 11 (2), 144–152.

Soulignac, F., Lemmin, U., Ziabari, S.M.H., Wynn, H.K., Graf, B., Barry, D.A., 2021. Rapid changes in river plume dynamics caused by advected wind-driven coastal upwelling as observed in Lake Geneva. Limnol. Oceanogr. 66, 3116–3133. https://doi.org/10.1002/lno.11864.

Umlauf, L., Lemmin, U., 2005. Interbasin exchange and mixing in the hypolimnion of a large lake: The role of long internal waves. Limnol. Oceanogr. 50, 1601–1611. https://doi.org/10.4319/lo.2005.50.5.1601.

Vallis, G.K., 2017. Atmospheric and Oceanic Fluid Dynamics: Fundamentals and Large-Scale Circulation, 2nd ed. Cambridge University Press, Cambridge. doi:10.1017/9781107588417.

van Sebille, E., Griffies, S.M., Abernathey, R., Adams, T.P., Berloff, P., Biastoch, A., Blanke, B., Chassignet, E.P., Cheng, Y., Cotter, C.J., Deleersnijder, E., Döös, K., Drake, H.F., Drijfhout, S., Gary, S.F., Heemink, A.W., Kjellsson, J., Koszalka, I.M., Lange, M., Lique, C., MacGilchrist, G.A., Marsh, R., Mayorga Adame, C.G., McAdam, R., Nencioli, F., Paris, C.B., Piggott, M.D., Polton, J.A., Rühs, S., Shah, S.H. A.M., Thomas, M.D., Wang, J., Wolfram, P.J., Zanna, L., Zika, J.D., 2018. Lagrangian ocean analysis: Fundamentals and practices. Ocean Model. 121, 49–75. https://doi.org/10.1016/j.ocemod.2017.11.008.

van Senden, D.C., Imboden, D.M., 1989. Internal seiche pumping between sill-separated basins. Geophys. Astrophys. Fluid Dyn. 48, 135–150. https://doi.org/10.1080/03091928908219530.

Voudouri, A., Avgoustoglou, E., Kaufmann, P., 2017. Impacts of observational data assimilation on operational forecasts. In: Karacostas, T., Bais, A., Nastos, P. (Eds.), Perspectives on Atmospheric Sciences. Springer, Cham, pp. 143–149. https://doi.org/10.1007/978-3-319-35095-0_21.

Wanner, H., Furger, M., 1990. The Bise - Climatology of a regional wind north of the Alps. Meteorol. Atmos. Phys. 43, 105–115. https://doi.org/10.1007/BF01028113.

Winant, C.D., 2004. Three-dimensional wind-driven flow in an elongated, rotating basin. J. Phys. Oceanogr. 34, 462–476. https://doi.org/10.1175/1520-0485(2004)034<0462:TWFIAE>2.0.CO;2.

Woolway, R.I., Kraemer, B.M., Lenters, J.D., Merchant, C.J., O'Reilly, C.M., Sharma, S., 2020. Global lake responses to climate change. Nat. Rev. Earth Environ. 1, 388–403. https://doi.org/10.1038/s43017-020-0067-5.